

# Late Holocene structural style and seismicity of highly transpressional faults in southern Haiti

Jiannan Wang, Paul Mann, Robert R. Stewart

Department of Earth and Atmospheric Sciences, University of Houston, Houston, Texas, USA.

## Key Points:

- First high-resolution sonar surveys of two actively ~~deformed~~-deforming lakes in Haiti.
- High degree of regional, tectonic transpression is partitioned by *en echelon* thrust faults and associated folds adjacent to a major strike-slip, plate boundary fault.
- ~~Estimates of relative ages of deformation of major strike-slip faulting and *en echelon* thrusts from deformed and undeformed lake sediments.~~ 3D deformation model integrates patterns of 2010 coseismic uplift, aftershock distribution, and mapped geologic structures.

14      **Abstract**

15      The devastating 2010 Haiti earthquake ( $M_w$  7.0) was caused by rupture of the Léogâne,  
 16      blind, thrust fault located 5 km north of the ~~main, Caribbean-Gonâve plate boundary, a~~  
 17      1200 km-long, left-lateral, Enriquillo-Plantain Garden fault zone (EPGFZ). Unexpect-  
 18      edly, the EPGFZ ~~, which~~ remained largely quiescent or slightly reactivated during the  
 19      2010 earthquake, ~~although~~. However, the EPGFZ still formed a boundary between a  
 20      coseismically uplifted lowland north of the EPGFZ and a subsided area in the highlands  
 21      south of the fault. Here, we use high-resolution sonar data from two, Haitian lakes that  
 22      straddle the EPGFZ and its northern flank to demonstrate the presence of a 10 – 15 km-  
 23      wide, 120 km-long, late Holocene fold-thrust belt which deforms clastic, lowland basins  
 24      along the northern edge of the EPGFZ. In the eastern part of the study area, sonar re-  
 25      sults from Lake Azuey show that the linear trace of the EPGFZ cutting the Holocene lake  
 26      bed is more deeply buried and less active than the adjacent, newly discovered, northwest-  
 27      striking, northeast-dipping Jimani thrust fault that is part of the adjacent ~~transpressional~~  
 28      transpressional belt of *en echelon* ~~thrust-and-fold~~thrusts and folds. This structural relation-  
 29      ship between a less active EPGFZ and more recently active, transpression-related Jimani  
 30      thrust is remarkably similar to the 2010 epicentral area 70 km to the west between the less  
 31      active EPGFZ and seismogenic Léogâne thrust during the 2010 Haiti earthquake. In this  
 32      complex transpressional zone, we propose that coseismic deformation alternates at recur-  
 33      rence intervals of centuries between oblique, transpression-related structures (Léogâne,  
 34      Jimani, and Trois Baies blind thrusts) and the main strike-slip, plate boundary fault zone  
 35      (EPGFZ).

36      **1 Introduction and tectonic setting of the 2010 Haiti earthquake**

37      On January 12, 2010, a  $M_w$  7.0 earthquake struck the densely populated, greater  
 38      Port-au-Prince region of south-central Haiti and caused widespread destruction with over  
 39      230,000 fatalities and an estimated 10 billion dollars damage [Prentice *et al.*, 2010; Bil-  
 40      ham, 2010; Paultre *et al.*, 2013; Kocel *et al.*, 2016] (Figure 1). Multidisciplinary, geolog-  
 41      ical and geophysical studies ~~of about~~ the 2010 epicentral area of south-central Haiti have  
 42      been done, including: 1) coseismic, coral reef uplift observation along a 50 km-long area  
 43      of coastline in the epicentral region combined with fault modeling [Hayes *et al.*, 2010];  
 44      2) coseismic, vertical ground motion from radar interferometry [Hashimoto *et al.*, 2011];  
 45      3) high-resolution, surface-fault-trace mapping using Light Detection And Ranging (LI-

46 DAR) and targeted field studies [Cowgill *et al.*, 2012]; 4) Global Positioning System (GPS)  
 47 and 2010 aftershock-based studies and modeling of pre-, syn-, and post-2010 earthquake  
 48 crustal motions [Calais *et al.*, 2010; Nettles and Hjörleifsdóttir, 2010; Symithe *et al.*, 2013;  
 49 Douilly *et al.*, 2013, 2015]; 5) ground-based studies of Holocene scarps including coseis-  
 50 mic ground fractures and late Quaternary scarps of the EPGFZ that remained unaffected  
 51 by 2010 fault breaks [Prentice *et al.*, 2010; Koehler and Mann, 2011; Rathje *et al.*, 2014;  
 52 Saint Fleur *et al.*, 2015]; 6) ground-based, near-surface, geophysical surveys of buried  
 53 faults activated during the 2010 earthquake [Kocel *et al.*, 2016]; 7) near-coast surveys of  
 54 submarine extensions of faults active in 2010 [Hornbach *et al.*, 2010; Mercier de Lépinay  
 55 *et al.*, 2011]; and 8) deepwater, marine surveys and coring to determine the recurrence in-  
 56 terval of major earthquakes based on anomalous sedimentary deposits related to shaking  
 57 and increased erosion [McHugh *et al.*, 2011].

58 The consensus from these previous, on- and offshore, multidisciplinary studies is  
 59 that the 2010 earthquake ruptured two, previously unrecognized west- to northwest-striking  
 60 thrust faults located 2 to 5 km north of the 1200 km-long, left-lateral, Enriquillo-Plantain  
 61 Garden fault zone (EPGFZ) that forms a major, plate boundary between the Caribbean  
 62 plate to the south and the Gonâve microplate to the north [Mann *et al.*, 1995; Calais *et al.*,  
 63 2010; Benford *et al.*, 2012; Corbeau *et al.*, 2016] (Figure 1A, B). These two thrust thrusts  
 64 are separated by 6 km and include: 1) the subaerial, 8 km-long, blind, Léogâne thrust  
 65 fault located 5 km north of the EPGFZ and trending at an angle of 8° to the EPGFZ [Calais  
 66 *et al.*, 2010; Douilly *et al.*, 2013, 2015]; and 2) the submarine, 20 km-long Trois Baies  
 67 thrust fault located 2 km north of the EPGFZ and trending at an angle of 20° [Mercier de  
 68 Lépinay *et al.*, 2011; Symithe *et al.*, 2013] (Figure 1B, C).

69 Despite the proximity of the Léogâne and Trois Baies thrust to the neighboring  
 70 EPGFZ, the EPGFZ remained largely quiescently quiescent and outside the zone of maxi-  
 71 mum, coseismic uplift and ground shaking and aftershocks related to the 2010 earthquake  
 72 [Nettles and Hjörleifsdóttir, 2010]. The centroid moment tensor (CMT) mechanism of the  
 73 main 2010 shock shows a primarily strike-slip motion, with a small component of reverse  
 74 motion, on a steeply north-dipping nodal plane [Nettles and Hjörleifsdóttir, 2010; Douilly  
 75 *et al.*, 2013]. Finite element modeling [Douilly *et al.*, 2015] suggests that Léogâne fault  
 76 buried beneath at least 1 km of overlying undeformed clastic sediment in the area north  
 77 of the EPGFZ absorbed most of the energy of the northwest-southeast northeast-southwest  
 78 compression along obliquely-striking, high-angle (21°-70° dipping) reverse fault planes;

79 ~~leaving significantly increasing but~~. For this reason, there was insufficient stress to trig-  
 80 ger ~~a~~slip during the 2010 ~~coseismic slip on the adjacent earthquake on the~~ EPGFZ 5 km  
 81 to the south (Figure 1B). Previous GPS surveys ~~by show~~ [Calais *et al.*, 2010, 2016] along  
 82 this area of the EPGFZ display vectors at almost right angles to these obliquely-striking  
 83 thrusts and consistent with their preferred reactivation (Figure 1A, B).

84 Aftershock studies following the 2010 earthquake by Douilly *et al.* [2013, 2015]  
 85 showed that the EPGFZ moved slightly at depth and acted as a 6 km-long, east-west and  
 86 sub-vertical, connecting fault segment that transmitted seismogenic motion between the  
 87 obliquely-trending, ~~south-dipping north-dipping~~, Léogâne fault in the east and the more  
 88 obliquely-trending, ~~northeast-dipping southwest-dipping~~ Trois Baies fault in the west (Fig-  
 89 ure 1B). However, post-earthquake geologic reconnaissance revealed no surface ground  
 90 breaks along the proposed onland areas of EPGFZ ~~motion~~ in the epicentral region of the  
 91 earthquake [Prentice *et al.*, 2010; Koehler and Mann, 2011; Rathje *et al.*, 2014]. A more  
 92 recent study by Saint Fleur *et al.* [2015] proposed previously, unrecognized, 2010 coseis-  
 93 mic groundbreaks along the obliquely-trending Lamentin thrust 11 km east of the epicen-  
 94 tral area near the city of Port-au-Prince (Figure 2A).

95 ~~Oblique, en echelon~~ En echelon thrusts spacing at distances of 1-8 km along the  
 96 main strike-slip fault, obliquely intersect the main strike-slip fault at angles of 30° ~~–~~  
 97 45°~~and~~. These structures strike northwestward away from the EPGFZ with individual  
 98 oblique, fault lengths extending into the deeper basins at distances of 4-29 km (Figure 2A,  
 99 *Figure 3*). As a result of this distinctive and regular intersecting fault geometry between  
 100 these oblique thrusts and the linear ~~and continuous~~ EPGFZ, earthquake rupture initiat-  
 101 ing on an oblique thrust, as seen for the Léogâne fault in 2010, is likely confined to that  
 102 vicinity and may not connect with other oblique thrusts or even the EPGFZ itself [Douilly  
 103 *et al.*, 2013, 2015].

104 Coseismic deformation along a large transpressional strike-slip fault, such as the  
 105 EPGFZ ~~and Septentrional~~ [Calais *et al.*, 2002] in Hispaniola or the San Andreas fault  
 106 zone in California [Segall and Lisowski, 1990], either is accommodated by slip and ma-  
 107 jor earthquakes on the main, strike-slip plate boundary fault, or is accommodated by the  
 108 oblique, *en echelon* thrusts adjacent to the main fault, or is accommodated by both sets of  
 109 faults (cf. compilation of types of destructive earthquakes in transpressional settings by  
 110 Hayes *et al.* [2010]). Motions on distributed, *en echelon* thrusts do not necessarily spare

111 or reduce coseismic rupture on the main strike-slip fault because the *en echelon* and main  
 112 strike-slip fault remain separate fault planes, and the main strike-slip fault could continue  
 113 to accumulate strain. In an extreme case, plate motions become increasingly transpres-  
 114 sional as seen in the case of the EPGFZ as manifested in the obliquity of GPS vectors  
 115 relative to the strike of the EPGFZ (Figure 1A, B) or in a restraining bend setting or dur-  
 116 ing the plate reorganizations. In ~~this~~these settings, the *en echelon*, oblique thrusts might  
 117 assume more and more plate-edge strain to the point that the plate boundary behaves more  
 118 like a ~~thrust belt~~broad, thrust boundary and less like a ~~narrow~~ strike-slip boundary.

119 These oblique and *en echelon* thrust faults in transpressional settings, including large  
 120 restraining bends ~~like as in~~ Hispaniola, potentially nucleate “uncharacteristic earthquakes”  
 121 of varying recurrence intervals and sizes that are distinct from the recurrence intervals  
 122 and sizes of the adjacent but independent strike-slip fault [Fielding *et al.*, 2013]. Restraining  
 123 bend areas like Hispaniola can lead to the generation and increased activities on more  
 124 favorably and obliquely oriented folds and thrusts whose coseismic rupture might alter-  
 125 ate with much longer ruptures along the adjacent strike-slip fault. The number of these  
 126 *en echelon*, ~~thrust faults~~thrust faults, in restraining bend setting, can be large at observed  
 127 ~~spacing~~spacings of 5-10 km ~~along~~dispersed along the trend of strike-slip faults that may  
 128 be hundreds of kilometers in total length. For this reason, the identification of oblique  
 129 ~~thrusts in~~en echelon sets~~thrusts~~, especially when buried or “blind”, can be challenging,  
 130 ~~along with~~assessing their role inwith seismogenesis within a broad plate boundary ~~and~~  
 131 ~~their recurrence intervals pose a major challenge for seismic hazard assessment in areas of~~  
 132 ~~regional transpression like Hispaniola~~ [Frankel *et al.*, 2011].

## 133 2 Objectives and methods

134 ~~The objective of this paper is to better integrate the geologic structure of the~~ 120  
 135 ~~km-long study area, that parallels the trace of the EPGFZ and includs the 2010 epicentral~~  
 136 ~~area, using a wealth of geologie, geophysics, GPS, radar interferometry, aftershock, and~~  
 137 ~~modeling studies, most of which has been colleeted since the 2010 earthquake. Our main~~  
 138 ~~objective is to use these information to structurally characterize the 10-15 km wide, belt of~~  
 139 ~~late Holocene, transpressional deformation that forms a laterally persistent, deformed belt~~  
 140 ~~along the inland, Cul-de-Sac intermontane basin in the east and the low-relief coastal plain~~  
 141 ~~along Port-au-Prince bay and the Canal du Sud to the west~~ 1B. In particular, we focus  
 142 ~~on the identifying a family of en echelon thrusts, whose curvilinear strikes area are very~~

143 similar to the Léogâne thrust now known to be responsible for most of the energy release  
 144 and coseismic uplift during the 2010 Haiti earthquake (Figure 1B, Figure 2A).

145 **2.1 Study area**

146 This elongate, belt of transpressional deformation associated with *en echelon* thrusts  
 147 occupies a topographically-low, densely populated Cul-de-Sac basin underlain by poorly  
 148 consolidated clastic sedimentary rocks ranging in age from Miocene to ~~recent~~ Recent  
 149 [Massoni, 1955; Mann *et al.*, 1995; Terrier *et al.*, 2014; Saint Fleur *et al.*, 2015]. In east-  
 150 ernmost Haiti, this belt is overlain by the shallow (33 m-deep), 138 km<sup>2</sup>, brackish  
 151 Lake Azuey near the border separating Haiti from the Dominican Republic [Wright *et al.*,  
 152 2015; Piasecki *et al.*, 2016]. Lake Enriquillo to the east is a larger, shallow (52 m-deep),  
 153 346 km<sup>2</sup>, hypersaline, sub-sealevel lake located entirely in the Dominican Republic and  
 154 separated from Lake Azuey by the eastward continuation of the same transpressional belt  
 155 parallel and north of the EPGFZ in the Cul-de-Sac valley [Mann *et al.*, 1995] (Figure 1B).

156 In the western part of our study area, the more transtensional segment of the EPGFZ  
 157 is overlain by the shallow 42.8 m-deep, 14 km<sup>2</sup>, freshwater Lake Miragoâne (Figure 1B). All  
 158 three of these shallow, inland, lakes experience variations up to 13 ~~meters~~ m in their sur-  
 159 face elevations due to annual to decadal changes in climate and rainfall amounts including  
 160 extreme rainfall associated with hurricanes [Wright *et al.*, 2015; Piasecki *et al.*, 2016; Mok-  
 161 nationian *et al.*, 2017; Rico, 2017].

162 **2.2 Objectives**

163 The main goal of this paper are to better integrate the geologic structure of the  
 164 120 km-long study area, which parallels the trace of the EPGFZ and includes the 2010  
 165 epicentral area, using a wealth of geologic, geophysics, GPS, radar interferometry, aftershock,  
 166 and modeling studies, most of which has been collected since the 2010 earthquake. Our  
 167 primary objective is to use these information to structurally characterize the 10-15 km-wide,  
 168 belt of late Holocene, transpressional deformation that forms a laterally-extensive, deformed  
 169 belt along the inland, Cul-de-Sac intermontane basin in the east and the low-relief coastal  
 170 plain along Port-au-Prince bay and the Canal du Sud to the west (Figure 1B). In particular,  
 171 we focus on the identifying a family of *en echelon* thrusts, whose curvilinear strikes area  
 172 are very similar to the Léogâne thrust now known to be responsible for most of the energy

173 release and coseismic uplift during the 2010 Haiti earthquake [Calais *et al.*, 2010; Douilly  
 174 *et al.*, 2013, 2015] (Figure 1B, Figure 2A).

175 **2.3 Survey design**

176 In order to understand the geologic and structural styles of transpression within this  
 177 belt, including the age relations between deformation in the north-flanking belt and the  
 178 EPGFZ itself, we collected a total of 94 km of high-resolution (2-10 kHz) sonar profiles  
 179 in 2014 from the 138 km<sup>2</sup>, brackish Lake Azuey (Figure 2A, B) and 37 km of profiles  
 180 from the 14 km<sup>2</sup>, fresh-water Lake Miragoâne (Figure 1B). The EPGFZ strikes through  
 181 both of the lakes, so 80% of our grid lines on Lake Azuey and 90% of our grid survey  
 182 lines on Lake Miragoâne was dedicated to the across fault-strike, north-south profiles (Figure 1B).

183 The average speed of the boat towing the sonar was 3 knots, and we used a sonar  
 184 pulse rate of 4 per second. Our 2-10 kHz sonar frequency range gives sub-bottom layer  
 185 resolution of about 10 cm. These surveys were the first sonar surveys in Haitian lakes.  
 186 Both lakes straddle the projected active trace of Haiti's EPGFZ and its adjacent, transpres-  
 187 sional fold-thrust belt, therefore provide new constraints on the location, structural style,  
 188 and timing of deformation within both structural provinces. We incorporate these lake  
 189 data with previous geologic mapping, geophysical observations related to the 2010 earth-  
 190 quake, and regional information on plate motions in this region (Figure 1B).

191 **3 Tectonic setting of transpressional deformation in south-central Haiti including  
 192 unresolved tectonic and structural questions**

193 **3.1 Previous strike-slip deformational model vs. Haiti thrust belt deformational  
 194 model**

195 There are two regional structural models to explain the present-day structure of the  
 196 broad, 250 km-wide zone of transpression spanning the entire width of the island of His-  
 197 paniola.

198 **3.1.1 Strike-slip, regional structural model**

199 The first is the strike-slip-dominated model, driven by oblique motion and trans-  
 200 pression between the thick and buoyant Bahama-Bahamas platform on the North Amer-  
 201 ica plate, the Caribbean plate, and the Gonâve plate-microplate [Mann *et al.*, 1995; Dolan

et al., 1998; Mann et al., 2002; Calais et al., 2002, 2016] (Figure 1A, B). Structures and tectonic geomorphology formed in this 250 km-wide, transpressional-transpressional zone include: 1) GPS studies [Calais et al., 2002, 2010; Hayes et al., 2010; Symithe et al., 2013; Douilly et al., 2013, 2015] reveal strain partitioning along the EPGFZ and the subparallel Septentrional strike-slip fault zone along the north side of the island as known from GPS studies; 2) as (which is the plate boundary between North Hispaniola microplate and Gonâve microplate) (Figure 1A). As a result of transpression, the central Hispaniola has the highest topography, up to 3 km, in all of the northern Caribbean region; 3) The left-lateral strike-slip rupture of the EPGFZ in the 18th century inferred from historical earthquakes [Bakun et al., 2012] with average left-lateral offset amounts of 1.3 – 3.3 m as expressed along offset streams of the EPGFZ [Prentice et al., 2010] and by left-lateral, channel offsets of 7 – 8 m along stream channels by the Septentrional fault zone; 4) [Prentice et al., 1993; Leroy et al., 2015]. Saint Fleur et al. [2015]'s study indicates the folding and thrusting of 10 – 15 km-wide belt of Miocene to Quaternary rock adjacent to the EPGFZ; and 5) In addition, Mann et al. [2002]; Grindlay et al. [2005]; Kroehler et al. [2011] suggest a strong, southwestward, backthrusting of the Gonâve microplate, in southern Hispaniola in Haiti and Dominican Republic to the southwest onto the Caribbean plate (Figure 1B, C). Southwestward backthrusting of Hispaniola is manifested by the accretionary wedges present along the Muerto trench south of the Dominican Republic [Bien-Aimé Momplaisir, 1986; Bruña et al., 2009] (Figure 1B) and along the southern margin of Haiti (South Haiti accretionary prism [Bien-Aimé Momplaisir, 1986] (Figure 1C), along with the associated, localized, negative gravity anomaly associated with plate flexure under a thrust load [Mann et al., 2002; Bruña et al., 2009] (Figure 1A)).

### 3.1.2 Criticisms of the strike-slip, regional structural model

Two criticisms have been proposed for the strike-slip model. First, Corbeau et al. [2016] has questioned whether the predictions of the GPS-based block models, which predict significant shortening, are accurate in that little transpression-related shortening can be observed from regional seismic profiles in the offshore area of the Gulf of Gonâve north of the southern peninsula of Haiti, or in the area of the Jamaica Passage east of Haiti. Second, Symithe and Calais [2016] have proposed that there is no geologic evidence for a continuation of the EPGFZ east of latitude 72.27°W in the eastern Cul-de-Sac Valley, Lake Azuey and Lake Enriquillo in the Dominican Republic (Figure 1B). Instead,

234 *Symithe and Calais* [2016] propose that large rates of north-south shortening predicted  
 235 from GPS block models is taken up entirely by low-angle thrust structures in the east-  
 236 ern Cul-de-Sac and Enriquillo Valleys that were modeled using GPS data as part of their  
 237 study.

238 ***3.1.3 Trans-Haitian fold-and-thrust belt regional structural model***

239 The Trans-Haitian fold-and-thrust belt model originated with a study by *Pubellier*  
 240 *et al.* [2000], who proposed a low-angle southwestward-verging fold-and-thrust belt along  
 241 the southwestern edge of the central Hispaniola block. The thrust front of this feature was  
 242 thought to be actively propagating from the main Trans-Haitian fold-and-thrust belt, lo-  
 243 cated in the Chaîne des Matheux ~~, (Figure 1B, Figure 2A)~~, southwestward into the area  
 244 of the Léogâne plain and the Cul-de-Sac basin ~~, further more, emerging into, as what we~~  
~~are proposing in this paper, the transpressional belt along the northern flank of the EPGFZ~~  
 245 (Figure 2A, B). *Pubellier et al.* [2000] proposed that the EPGFZ originally formed as a  
 246 left-lateral strike-slip fault, but became inactive in the late Miocene when deformation in  
 247 southern Hispaniola became compressional and the Trans-Haitian fold-and-thrust belt had  
 248 propagated into the southern area of the Cul-de-Sac basin and Léogâne plain, where it  
 249 emerged or “daylighted” to form the *en echelon*, convergent structures (compiled on the  
 250 map in Figure 2). *Pubellier et al.* [2000] also proposed that the EPGFZ was reactivated  
 251 as a normal fault in the Quaternary as a result of crustal loading of the southern, foreland  
 252 area by the overthrusting Trans-Haitian fold-and-thrust belt.

254 Following the 2010 earthquake and the recognition of the north-dipping blind Léogâne  
 255 thrust fault, *Calais et al.* [2010] proposed that this fault is the leading edge of the Trans-  
 256 Haitian fold-and-thrust belt rather than being an *en echelon* thrust genetically linked to the  
~~257 EPGFZ, as we propose in this paper based on the geologic data compiled on Figure 2A,~~  
 258 **B.** In the interpretation proposed by *Calais et al.* [2010], the northward dip of the Léogâne  
 259 thrust made it difficult to link its origin with the EPGFZ, whose dip had been established  
 260 in this area as a vertical to high angle ( $> 60^\circ$ ), south-dipping fault plane with evidence of  
 261 late Holocene, left-lateral offsets of drainages [*Prentice et al.*, 2010]. Moreover, *Symithe*  
 262 and *Calais* [2016] noted that Trans-Haitian fold-and-thrust belt regional model of *Pubel-*  
~~lier et al.~~ [2000] was more consistent with an increasing amount of GPS data supportive  
 263 of a larger magnitude, north-south shortening in central Hispaniola than with the existence

265 of an eastward extension of the left-lateral EPGFZ into the eastern part of Haiti and the  
 266 Dominican Republic (Figure 1B and Figure 2A).

267 **3.1.4 Criticisms of the Trans-Haitian fold-and-thrust belt, regional structural model**

268 First, *Mercier de Lépinay et al.* [2011] pointed out two problems with linking the  
 269 origin of the Léogâne thrust to the southwestward-propagating edge of the Trans-Haitian  
 270 fold-and-thrust belt: 1) the dip of the fault generating the main thrust, derived by *the*  
 271 *Mercier de Lépinay et al.* [2011], was more steeply dipping ( $64^\circ$ ) than expected for a blind  
 272 thrust at the leading edge of a fold-thrust belt; and 2) the orientation of the N84°E fault  
 273 plane of the main shock is significantly oblique to the N120°E-oriented leading edge of  
 274 the Trans-Haitian fold-and-thrust belt as proposed by *Pubellier et al.* [2000]. In this paper,  
 275 we discuss other inconsistencies with the zone of deformation north of the EPGFZ being  
 276 the result of southwestward propagation of the Trans-Haitian fold-and-thrust belt.

277 **4 New observations of the Late Holocene structural style along EPGFZ in southern**  
 278 **Haiti**

279 **4.1 Significance of *en echelon* thrusting and folding north and south of the EPGFZ**

280 The presence of a strike-slip fault at any scale is indicated by the presence of *en ech-*  
 281 *elon* arrays of thrust faults, normal faults, folds, fractures, dikes, and other linear features  
 282 in narrow, elongate zones [Sylvester, 1988]. On Figure 2A, we have compiled geologic in-  
 283 formation on *en echelon* folds and faults in a 10 – 15 km-wide zone of deformation along  
 284 both the northern and southern flanks of the EPGFZ. Folds form as fault propagation folds  
 285 along oblique *thrust* faults, vary from 1 to 8 km in lateral spacing; and deform Miocene  
 286 and younger fine to coarse-grained, basinal, and coastal plain rocks in the belt that is 10  
 287 – 15 km wide and extends parallel to the EPGFZ for 120 km (Figure 1B and Figure 2A).  
 288 Folds in Neogene clastic lithologies of the Cul-de-Sac basin contrast with more continuous  
 289 and longer wavelength, *en echelon* fold axes present in more massively-bedded Cretaceous  
 290 to Eocene rigid, basaltic, and carbonate lithologies exposed in the 2 km-high range south  
 291 of the EPGFZ, the Massif de Selle (Figure 2B). The trend of fold axes is similar to the  
 292 north and south of the EPGFZ (Figure 2B).

293 The *en echelon* distribution of complex Holocene folding and thrusting in the 10  
 294 – 15 km wide zone of deformation north of the EPGFZ is also reflected in the complex

pattern of 2010 coseismic and vertical deformation recorded by the interferogram from the 2010 epicentral area on the Léogâne plain west of the Cul-de-Sac basin [Hayes *et al.*, 2010; Hashimoto *et al.*, 2011; Bilham and Fielding, 2013] (Figure 2A). Douilly *et al.* [2013, 2015] and Kocel *et al.* [2016] use aftershocks and shallow geophysics to show that the 2010 Léogâne thrust fault and sub-parallel faults are overlain by at least one kilometer of undeformed and sub-horizontal strata.

#### 301           **4.2 Significance of curvilinear fold and thrust patterns in the transpressional belt 302           north of the EPGFZ**

303           The shaded relief DEM (digital elevation model) shown in Figure 2B reveals the  
304           curvilinear, *en echelon* fold morphologies that are defined by low, bedrock hills of Neo-  
305           gene sedimentary rocks exposed on the flat-lying Cul-de-Sac basin. These curvilinear fold  
306           axes can be related directly to a broad zone of left-lateral, simple shear produced along  
307           the sub-vertical and left-lateral EPGFZ based on several, basic observations seen on Fig-  
308           ure ~~figure2B: 1) the 2B. The~~ most prominent folds are present along the southern edge  
309           of the Cul-de-Sac basin within 15 km of the EPGFZ; ~~in~~. ~~In~~ contrast, the central and  
310           northern edges of the Cul-de-Sac basin exhibit no prominent folding even directly adja-  
311           cent to the base of Eocene-Miocene carbonate rocks forming the range [Pubellier *et al.*,  
312           2000] (Figure 2A); ~~2) as typical broad zones of shearing on the thick, sedimentary rocks  
313           as shown schematically in the inset of Figure 2B (modified from ). The map-view  
314           shapes of~~ fold axes along the southern margin of the Cul-de-Sac basin are asymptotic,  
315           or gently curve into east-west parallelism with the main trace of the EPGFZ along the  
316           southern edge of the Cul-de-Sac basin; ~~3) deeper, as broad zones of shearing of thick,~~  
317           ~~sedimentary basins (see the inset of Figure 2B; modified from Odonne and Vialon [1983]).~~  
318           ~~Deeper~~, structural depressions form in the zone of convergent intersection between the  
319           east-west-striking EPGFZ and the northwest-striking, secondary thrusts as seen in the  
320           southern part of Lake Azuey, where the lake bends from an east-west trend adjacent to  
321           the EPGFZ to a more northwest trend in the central and northern part of the basin (Fig-  
322           ure ~~figure2A, B); and 4) in our sonar mapping of Lake Azuey described below, we observed  
323           late Holocene lake sediments onlapping onto local highs of Eocene limestone of the bounding  
324           range along the northern edge of the lake with no evidence of late Holocene faulting or  
325           folding as observed with the EPGFZ along the southern edge of the lake (Figure 2A).~~

326        On a more regional scale, these observations form Lake Azuey are consistent with  
 327        the Canadian Superior 2D 2A, multi-channel seismic reflection profile (shown in Figure 1C),  
 328        that shows a lack of intensive deformation in the northern part of Port-au-Prince Bay, that  
 329        is the offshore, largely un-faulted and folded seaward extension of the Cul-de-Sac basin.  
 330        proposes that the Trans-Haitian fold-and-thrust belt exposed in the Chaine des Matheux  
 331        range north extends beneath the entire Cul-de-Sac and Port-au-Prince basins (Figure 2A,  
 332        B). In summary, our observations at this scale do not support the previous model by and  
 333        that folds and faults of the northern range are propagating southwestward beneath the zone  
 334        of *en echelon* faults and folds (Figure 2A, B).

335        **4.3 Geologic structure of the area of *en echelon* thrusts in the epicentral area on  
 336        the Léogâne fan-delta**

337        **4.3.1 Geologic structure of the Léogâne fan area**

338        A ~~cross-sectional~~cross-sectional profile of the 2010 epicentral area related to the ac-  
 339        tivation of two ~~,~~conjugate thrust faults was modified from aftershock data from *Douilly*  
 340        *et al.* [2013, 2015] is shown in Figure 3 (Line A–A'). Both faults are buried by about 1  
 341        km of late Quaternary sand and gravel of the Léogâne fan delta [*Kocel et al.*, 2016] and an  
 342        additional 1 km of Paleocene limestone. Aftershocks indicate that the main thrust event  
 343        ruptured a depth range of from 4 to 17 km beneath the ground surface [*Douilly et al.*,  
 344        2013, 2015]. The orientation of the Léogâne thrust based on gravity and uplift of coastal  
 345        features is east-west and parallel to recent near-surface breaks of the EPGFZ mapped in  
 346        the shallow, coastal zone adjacent to the Léogâne plain [*Hornbach et al.*, 2010]. Due to its  
 347        proximity to the EPGFZ, an east-west strike of the Léogâne thrust is predicted as this is  
 348        the area where *en echelon* folds and faults curve into an asymptotic orientation relative to  
 349        the main EPGFZ, as shown on Figure 2B.

350        A radar interferogram compiled on the structure map of Figure 2A revealed that the  
 351        2010 earthquake elevated the smaller folds of the Léogâne fan-delta north of the EPGFZ,  
 352        yet produced coseismic subsidence in the 1.4 km-high, less complexly deformed, mountain  
 353        range south of the EPGFZ ~~to the south~~[*Hashimoto et al.*, 2011] (Figure 2A). This para-  
 354        dox can be simply explained by the northward dip of the seismogenic Léogâne fault that  
 355        elevated the basinal area to the north (hanging wall of the Léogâne fault) and depressed

356 the mountainous area to the south (footwall block of the Léogâne fault (line A–A' in Fig-  
 357 ure 3).

358 **4.3.2 Geologic structure of the ~~greater~~-Port-au-Prince urban area compared to the**  
 359 **Léogâne epicentral area**

360 A similar pattern of deformation is observed in Port-au-Prince urban area where  
 361 the central and northern edge of the Cul-de-Sac basin is almost undeformed [Massoni,  
 362 1955; Cox *et al.*, 2011; McHugh *et al.*, 2011; Saint Fleur *et al.*, 2015] (Line B-B' in Fig-  
 363 ure 3). The cross section taken from workers, who were mapping 60 years ago when  
 364 the city was smaller and the geology was less obscured by urbanization, shows two large  
 365 thrusts, a range-bounding thrust along the southern edge of the city, and a north-dipping  
 366 northeast-dipping thrust, the Dumay thrust, that elevates a broad outcrop zone of north-  
 367 dipping, Neogene sedimentary rocks on which the northern part of the city is built [Rathje  
 368 *et al.*, 2014]. The 50° northeast dip of the Dumay thrust is similar to the 70° northeast dip  
 369 of the Léogâne thrust to the west known from aftershocks [Douilly *et al.*, 2013, 2015],  
 370 although the dip of the Dumay thrust reverses to a southwest dip as it approaches the  
 371 EPGFZ (Figure 2A, B). On the cross section B-B' in Figure 3, we have schematically  
 372 indicated areas that are elevated as a result of the northward dip of the Dumay thrust  
 373 and the depression of the area to the south of the EPGFZ in the highlands south of the  
 374 EPGFZ. If a future earthquake occurred along the north-dipping, *en echelon* thrust faults  
 375 in the Port-au-Prince are-area (Line B-B' in Figure 3) or Lake Azuey area (Line C-C' in  
 376 Figure 3) a similar uplift phenomenon probably would occur where the lowlands are up-  
 377 lifted and the adjacent mountains subside.

378 **4.3.3 Geologic structure of the Lake Azuey area**

379 Structural cross-sections (Figure 3) from this and the previous works (Line A-A' and  
 380 In the Lake Azuey area, we mapped a linear and east-west striking fault trace in deformed  
 381 Holocene sediments along the projected trend of the landward traces of the EPGFZ both  
 382 east and west of Lake Azuey (Figure 4 and Figure 5A, B). Integrated with previous land  
 383 mapping of the EPGFZ [Bourgueil *et al.*, 1988; Mann *et al.*, 1995; Prentice *et al.*, 2010;  
 384 Cowgill *et al.*, 2012], we interpret this linear east-west striking feature in Lake Azuey as  
 385 a 5 m-wide and continuous trace of the EPGFZ which we can follow westward to the  
 386 EPGFZ locality at Dumay, about half way between Lake Azuey and Port-au-Prince, which

387 was previously described and dated as a 6 m-long, left-lateral offset of a late Holocene  
 388 stream channel [Cowgill *et al.*, 2012] (locates at red circle, which is labeled as Dumay  
 389 in Figure 2A). The structural cross sections in this area taken from the previous studies  
 390 [Massoni, 1955; Mann *et al.*, 1995; Douilly *et al.*, 2015] indicate that the high-angle EPGFZ  
 391 co-exists with the adjacent thrusts that over-thrust from the south and north (Line B–B'  
 392 in Figure 3) along this 120 km-long zone of deformation adjacent to the EPGFZ (3). We  
 393 project this trace of the EPGFZ along a prominent fault valley at the town of Jimani that  
 394 separates Lakes Azuey and Enriquillo (Figure 2A and Figure 4). Sonar profiles (Figure 5A,  
 395 B) show that the oblique thrust faults share a similar orientation with other north-dipping  
 396 thrusts along the northern edge of most recent rupture of the EPGFZ is covered by about  
 397 0.7 m of Holocene sediment, suggesting that there has been late Holocene activity of the  
 398 EPGFZ along the southern edge of the EPGFZ. All three of these oblique thrust faults  
 399 shown on the cross sections deform rocks as young as Pliocene and Quaternary lake.

400 In our sonar survey of Lake Azuey From sonar data, we observed late Holocene lake  
 401 sediments onlapping onto local highs of Eocene limestone of the bounding range along the  
 402 northern edge of the EPGFZ (Figure 5). The sonar from southern Lake Azuey suggests  
 403 that the most prominent folds present adjacent to the EPGFZ become less prominent in  
 404 the central and northern parts of the lake (Figure 2B). These southern folds and thrusts  
 405 imaged in Lake Azuey define the transpressive belt along the EPGFZ observed in onshore  
 406 areas to the west. On the cross section C–C' in Figure 35C, we have schematically indi-  
 407 cated areas that are elevated as a result of the northward dip of the Jimani thrust and the  
 408 depression of the area to the south of the EPGFZ in the highlands south.

409 The structural cross-section (Figure 5C) of the Lake Azuey area and the previous  
 410 works [Massoni, 1955; Bourgueil *et al.*, 1988; Cox *et al.*, 2011; Douilly *et al.*, 2015] (Line  
 411 A–A' and B–B' in Figure 3) along this 120 km-long zone of deformation adjacent to the  
 412 EPGFZ show that the oblique thrust faults share a similar orientation with other northeast-dipping  
 413 thrusts along the northern edge of the EPGFZ. All three of these oblique thrust faults (the  
 414 Léogâne thrust in Line A–A', the Dumay thrust in Line B–B', and the Jimani thrust in  
 415 Figure 5C) shown on the cross sections deform rocks as young as Pliocene and Quaternary  
 416 [Saint Fleur *et al.*, 2015].

417 On a more regional scale, these observations from Lake Azuey are consistent with  
 418 the multi-channel seismic reflection profile (named as Canadian Superior 2D and shown

419 in Figure 1C), that shows a lack of intensive deformation in the part of Port-au-Prince  
 420 Bay, that is the offshore, largely un-faulted and folded seaward extension of the Cul-de-Sac  
 421 basin [McHugh *et al.*, 2011]. Pubellier *et al.* [2000] proposes that the Trans-Haitian fold-and-thrust  
 422 belt exposed in the Chaine des Matheux range extends beneath the entire Cul-de-Sac and  
 423 Port-au-Prince basins (Figure 2A, B). In summary, our observations at this scale do not  
 424 support the previous model by Pubellier *et al.* [2000] and Calais *et al.* [2010] that folds  
 425 and faults of the northern range are propagating southwestward beneath the zone of *en echelon*  
 426 faults and folds (Figure 2A, B).

#### 427 4.4 Subsurface stratigraphy of Lake Azuey and Lake Enriquillo and paleoseis- 428 mic estimates of the relative timing of recent earthquakes on the EPGFZ and 429 secondary, *en echelon* thrust faults

430 Our objective is to determine the relative age of the EPGFZ and its adjacent zone  
 431 of fold-and-thrust deformation using the sonar profiles from Lakes Azuey and Enriquillo  
 432 (Figure 6A). Both previous coring Previous coring, both in Lake Enriquillo [Rios *et al.*,  
 433 2013] which was tied to the onshore stratigraphic studies [Taylor *et al.*, 1985; Rios *et al.*,  
 434 2013], and in Lake Miragoâne [Higuera-Gundy *et al.*, 1999] have has established the  
 435 late Holocene to include the upper 5 m and 7 meters of both lakesm sedimentary history,  
 436 respectively.

437 In Lake Enriquillo, a sonar survey similar to ours was conducted in 2013 [Rios  
 438 *et al.*, 2013]. Mapping in both lakes revealed the presence of the east-west strands of  
 439 the EPGFZ that are collinear with onshore scarps both east and west of Lake Azuey (Fig-  
 440 ure 2, Figure 6, and Figure 4) and east and west of Lake Enriquillo [Mann *et al.*, 1995;  
 441 Rios *et al.*, 2013]. These east-west fault strands abruptly truncate the trends of folds in the  
 442 ranges south of the lake (Figure 4).

443 In Lake Enriquillo, a sonar survey similar to ours was conducted in 2013. The  
 444 sonar events, which are interpreted as stratigraphic features, from Lake Azuey and Lake  
 445 Enriquillo (Line B1 and Line L19 correlate convincingly (Figure 6B). Given the small  
 446 distance separating the two lakes (about 4 km); the similarity of the stratigraphic pro-  
 447 files; and the same amount of sediment above the EPGFZ; it is reasonable to suggest that  
 448 Lake Azuey and Lake Enriquillo share the same sedimentation history as well as the same  
 449 structural style and seismicity related to the EPGFZ and its oblique, thrust faults.

450 The EPGFZ in both Lake Enriquillo and Lake Azuey is buried by 0.7 m of sedi-  
 451 ments. According to coring studies in the Dominican Republic [Taylor *et al.*, 1985; Rios  
 452 *et al.*, 2013], the 5.2 m thickness of the latest lake stage (2 ka BP to present) gives a re-  
 453 cent Holocene average sedimentation rate of 2.6 mm/yr (Figure 6B). Using the average  
 454 sediment rate, the most recent rupture of the EPGFZ would be dated to some 270 years  
 455 ago. Given the historical earthquake records [Bakun *et al.*, 2012], we suggest that the most  
 456 recent rupture of the EPGFZ ~~is corresponds to the historical events of~~ October or Novem-  
 457 ber ~~of~~ 1751, and the deformed sediments in Lake Azuey are of Holocene age.

#### 458 **4.5 Mapping of the EPGFZ trace from sonar data in deformed lake sediments of 459 Lake Azuey, Haiti**

460 ~~In the Lake Azuey area (Figure 2A), we mapped a linear and east-west striking fault~~  
 461 ~~trace in deformed Holocene sediments along with its landfall (Figure 6A, B and Figure 4).~~  
 462 ~~Integrated with previous land mapping of the EPGFZ, we interpret this linear east-west~~  
 463 ~~striking feature in Lake Azuey as a 5 m-wide and continuous trace of the EPGFZ which~~  
 464 ~~we can follow eastward to the EPGFZ locality at Dumay, about half way between Lake~~  
 465 ~~Azuey and Port-au-Prince, which was previously described and dated as a 6 m-long, left-lateral~~  
 466 ~~offset of a late Holocene stream channel (shown in Figure 2A).~~

467 ~~The structural cross sections in this area taken from the previous studies indicate~~  
 468 ~~that the high-angle EPGFZ co-exists with the adjacent thrusts that over-thrust from the~~  
 469 ~~south and north (Line B-B' in Figure 3). Sonar profiles from the southernmost area of~~  
 470 ~~Lake Azuey (Figure 5) show that the most recent rupture of the EPGFZ is covered by~~  
 471 ~~about 0.7 m of Holocene sediment, suggesting that there has been no recent activity of~~  
 472 ~~the EPGFZ. We project this trace of the EPGFZ along a prominent fault valley at the town~~  
 473 ~~of Jimani that separates Lakes Azuey and Enriquillo (Figure 2A and Figure 4).~~

#### 474 **4.5 Easternmost extent of the EPGFZ trace in Lake Enriquillo, Dominican Re- 475 public**

476 Based on both of our lake surveys combined with a previous survey of Lake En-  
 477 riquillo in the Dominican Republic [Rios *et al.*, 2013], and the previous geologic mapping  
 478 of the basinal and topographic corridor of the Cul-de-Sac basin in Haiti and the Enriquillo  
 479 basin in the Dominican Republic [Mann *et al.*, 1995; Mann, 1999], a first-order question

480 we pose is whether the EPGFZ extends as a continuous, strike-slip fault along the 120  
 481 km-long zone of deformation of Miocene and younger clastic rocks present between the  
 482 two lakes ([Figure 1B](#) and [Figure 6A](#)). The previous studies [*Saint Fleur et al.*, 2015;  
 483 *Symithe and Calais*, 2016] have proposed that the EPGFZ terminates as a strike-slip fea-  
 484 ture in the area south of Port-au-Prince. These studies further ~~propose~~[have proposed](#) that  
 485 transpressional plate motion in the eastern Cul-de-Sac basin and the Enriquillo Valley in  
 486 the Dominican Republic ([Figure 1B](#) and [Figure 6A](#)) is entirely accommodated along the  
 487 low-angle oblique-thrust structures that overthrust the southern edges of Lake Azuey and  
 488 Lake Enriquillo([Figure 1B](#) and [Figure 6A](#)).

489 A previous study of Lake Enriquillo by *Rios et al.* [2013] identified the break along  
 490 the northeastern edge of Cabritos Island in Lake Enriquillo, which aligns exactly with the  
 491 large east-western lineament extending eastward from our map area in Lake Azuey (Fig-  
 492 ure 6A). The sonar results from both lakes show that the EPGFZ extends to at least to  
 493 the eastern tip of Cabritos Island in the center of Lake Enriquillo, Dominican Republic  
 494 [*Mann et al.*, 1995](Figure 6A). This survey revealed a fault penetrating the youngest sed-  
 495 iment layer of Holocene age which is consistent with recent activity on this segment of  
 496 the EPGFZ (Figure 5A, B). ~~Therefor~~[Therefore](#), we conclude that this linear, late Holocene  
 497 strike-slip fault extends at 55 km (at least) to the eastern edge of Lake Enriquillo, where  
 498 the ~~recently documented~~[previously documented](#) [*Mann et al.*, 1995] uplift of the Holocene  
 499 reef fringes Lake Enriquillo.

## 5 Active tectonics of the area west of the 2010 epicentral zone in the western study 501 area: [Léogâne plain, Miragoâne basin, and their adjacent offshore area](#)

### 5.1 [The Trois Baies thrust fault, Canal du Sud, as a](#) termination structure for 502 the 2010 earthquake

504 The 2010 aftershock zone at the western and central part of our study area (Fig-  
 505 ure 7A) reflects the rupture along the northwest-striking, 20 km-long, submarine, Trois  
 506 Baies thrust fault that forms the western extension of the 10 – 15 km-wide, transpressional  
 507 zone north of the EPGFZ. As the Trois Baies fault is submarine, InSAR cannot be used  
 508 to assess its 2010 coseismic similarity with folding and thrusting along the Léogâne thrust  
 509 that affected the onshore, Léogâne plain (Figure [7A](#)).

510 However, the same basic structural elements of the Léogâne plain are also observed  
 511 for the Trois Baies thrust fault, which include the short distance (1 km) to the EPGFZ and  
 512 its steep ( $45^\circ$ ) but opposite (southwest) dip of the Trois Baies thrust fault (Figure 7A).  
 513 One of the most intense zones of coseismic, aftershock, ~~and coastal uplift~~ coastal uplift  
 514 [Hashimoto et al., 2011], and subsidence [Prentice et al., 2010] separates the oppositely-  
 515 dipping Léogâne and Trois Baies faults, and may represent complex deformation at a  
 516 transfer zone between the two faults (Figure 7A, B). The aftershock study of the Trois  
 517 Baies fault [Symithe and Calais, 2016] shows that ~~it~~ its thrust character and oblique orientation  
 518 in map view with the main EPGFZ is comparable to the cross sections of the eastern area  
 519 in Figure 3. ~~The~~ In the map view, the overall structure of this western part of the study  
 520 area mirrors the same ~~geometry of geometrical relationship between~~ the oblique thrusts  
 521 (such as the Trois Baies thrust fault) and the main EPGFZ as described at the eastern part  
 522 of the study area (Figure 2).

## 523 5.2 Structure of the Miragoâne pull-apart basin

524 In the onshore part of the western study area, Lake Miragoâne was interpreted as a  
 525 14 km<sup>2</sup> pull-part basin developed as a left-stepping, releasing bend on the EPGFZ paired  
 526 with the adjacent Tapion du Petit Goâve restraining bend 12 km to the east (Figure 7)  
 527 [Cowgill et al., 2012]. Bathymetry from our sonar data shows the maximum water depth  
 528 of Lake Miragoâne is 42.8 m (Figure 7B), which makes this ~~actively faulted~~ lake the deepest  
 529 [Higuera-Gundy et al., 1999] in the Caribbean region. The 30 m of recognizable stratig-  
 530 raphy (Figure 8A, B and C) from the sonar survey in Lake Miragoâne reveals a series  
 531 of deformational features including major east-west normal faults, minor thrust faults at  
 532 ~~deep depth~~ (some 20 m), and active folds at the lake bottom (Figure 8). The upper 7  
 533 m of the lake ~~sediment was sediments were~~ cored and dated ~~as-at~~ 10 ka at the bottom  
 534 of the core. ~~Extrapolating the~~ [Higuera-Gundy et al., 1999]. By applying the average  
 535 sedimentary rate from the core data to the chirp sonar trace, we can extrapolate the sed-  
 536 imation rate to the observed thickness of 30 m in the lake ~~allows and estimate~~ a min-  
 537 imum of ~~33 ka to be calculated~~ 43 ka for the age of the pull-apart basin on the EPGFZ.  
 538 Core measurements of the E/P (evaporation and precipitation ratio from the  $\delta^{18}\text{O}$  of ostra-  
 539 cod shells in the core sample) were undertaken [Higuera-Gundy et al., 1999] in the center  
 540 of Lake Miragoâne (Figure 9B). The core reveals that the uppermost part of the ~~sediment~~

541 is Holocene and sediments are Holocene to the latest Pleistocene lacustrine (Figure in age  
 542 (Figure 9A). Pollen data from the core indicate alternating dry and wet environments.

### 543 5.3 Ages and sedimentary cycles of the Miragoâne pull-apart basin

544 Comparing the core data with the sonar data, we can see the sediment layers from  
 545 drier climates (higher E/P) correlate with stronger acoustic reflectivity and vice versa  
 546 (Figure 9A). We applied a low-pass filter on the pollen log data (from the core acquired  
 547 by Higuera-Gundy et al. [1999] in the center of the lake) and found a strong correlation  
 548 between the pollen and sonar data (red curve in Figure 9B). To further investigate this in-  
 549 teresting correlation between the geochemical and geophysical data, we use the filtered  
 550 E/P log, considered as pseudo-acoustic impedance log, to generate a synthetic sonar re-  
 551 sponse (Figure 9B). The correlation is compelling which suggests that the depositional  
 552 environment influences the acoustic properties of the sediments and sonar response may  
 553 be a partial proxy for climatic processes. In another words, the sediment layers from drier  
 554 climates (higher E/P) have stronger acoustic reflectivity and vice versa. Combining the  
 555 correlation between the pollen log and the acoustic reflections from the chirp sonar data,  
 556 we can extend the sedimentary history of the upper 7 m from the log data to the entire  
 557 sonar data set. In the sonar profile, we find the most recent rupture in the lake is buried  
 558 by about 0.5 meter sediment (Figure 8B, C). The core dating result from Higuera-Gundy et al. [1999]  
 559 suggests the age of these rupture is about 300 years old. The historical document record  
 560 [Bakun et al., 2012] indicates a historical earthquake happened in this area in 1770. Con-  
 561 sidering the historical document record [Bakun et al., 2012], the dating of the core and  
 562 and the sonar interpretation in Lake Miragoâne suggest that the most recent rupture in this  
 563 lake is likely related to a the historic earthquake in 1770 [Bakun et al., 2012].

## 564 6 Discussion

### 565 6.1 Proposed 3D structural model for the 10 – 15 km-wide belt of transpressional 566 deformation along the northern edge of the EPGFZ

567 In summary, our lake studies, along with previous work, favor a model of a 10 –  
 568 15 km-wide transpressional zone that deforms thick, loosely-consolidated, Miocene to  
 569 recent clastic rocks in coastal, marine, and lake settings as shown in three dimensions  
 570 (Figure illustrated in three-dimensional block diagram (Figure 10). Moving from Lake

571 Azuey in the east to Lake Miragoâne in the west, the block diagram illustrates along-strike  
 572 changes observed in the dips of the thrust faults and obliquely orientation to the EPGFZ.  
 573 Fold axes north of the EPGFZ range from 3 to 20 km in length, and are sigmoidally re-  
 574 lated to the EPGFZ in map view (Figure 2A, B). Dip direction and amounts on these  
 575 thrust faults vary from north-dipping at 21° on the Jimani fault (**C–C'** in Figure 3, Fig-  
 576 ure 5C and Figure 10), south-dipping on the Lamentine fault [Saint Fleur *et al.*, 2015] at  
 577 40°, north-dipping at 70° on the Léogâne fault active during the 2010 earthquake (A–A' in  
 578 Figure 3, Figure 10), and south-dipping on the Trois Baies fault at 45° (Figure 10).

579 South of the EPGFZ, transpressional folding in more rigid Cretaceous basalts and  
 580 overlying Eocene limestone have ~~wavelengths ranging broader wavelengths~~ from  
 581 1 to 8 km ~~and a weak seismogenic deformation. On the other hand,~~ InSAR images of  
 582 the 2010 earthquake indicate smaller folds and more seismogenic deformation in the 10  
 583 – 15 km belt north of the EPGFZ~~as opposed to the broader folding and less seismogenic~~  
 584 ~~deformation south of the EPGFZ~~. This contrast is likely related to rock type with poorly  
 585 consolidated sedimentary rocks up to several kilometers north of the EPGFZ and more  
 586 consolidated carbonate rocks and basalts exposed in the highlands south of the EPGFZ  
 587 [*Mann et al.*, 1991] (Figure 2).

588 We propose that the folds north of the EPGFZ formed originally as conjugate thrust  
 589 faults, reflecting the northeast to southwest convergence indicated by GPS vectors and  
 590 highly transpressional character of the EPGFZ [Calais *et al.*, 2010]. Conjugate thrust faults  
 591 are common in thick, clastic sedimentary basins undergoing active, sub-horizontal short-  
 592 ening [Sibson, 2012], as documented in the  $M_w$  7.6 Chi-Chi Taiwan earthquake in 1999  
 593 [*Chen et al.*, 2002] or the  $M_w$  7.1 Kumamoto Japan earthquake in 2016 [*Lin and Chiba*,  
 594 2017]. Aftershocks north of the EPGFZ reflect the most recent phase of NE-SW shorten-  
 595 ing on the 70° dipping reverse fault planes [Nettles and Hjörleifsdóttir, 2010], along the  
 596 deeply buried Léogâne thrust fault, as shown in the cross-section of A–A' in Figure 3.

597 Our results, including the eastward extension of the EPGFZ into Dominican Republic,  
 598 support the “thick-skinned” strike-slip model for the deformation of Hispaniola region  
 599 as opposed to the southwestward propagation of the Trans-Haitian fold-and-thrust belt  
 600 proposed by .

601           **6.2 Analogy between the 2010 coseismic transpressional deformation in Haiti and**  
 602           **the 1989 Loma Prieta earthquake in northern California**

603           **6.3 Is the 2010 coseismic transpressional deformation in Haiti analogous to the**  
 604           **1989 Loma Prieta earthquake in northern California?**

605           A similar pattern of transpression in a restraining bend setting to Haiti has been  
 606           described for 1989  $M_w$  6.9 Loma Prieta earthquake [Marshall *et al.*, 1991] (Figure 11).

607           These aftershocks define a conjugate pair of reverse faults with the dominant motion on  
 608           the north-dipping fault plane.

609           Features compiled on the map from various sources include: 1) The selected GPS  
 610           vectors from relative to a fixed North America plate showing [UNAVCO (*University Nav-*  
 611           *star Consortium*), 2009] indicate the transpressional setting in a gentle restraining bend set-  
 612           ting; 2) inset map with cross-section of . In the inset map of Figure 11, the 1989 hypocen-  
 613           tral area showing the main shock (yellow star) and related aftershocks (red dots) along the  
 614           southwest-dipping San Andreas and Sargent faults from ; 3) documentation of the [Mar-  
 615           shall *et al.*, 1991] shows the steep (~ 61°) dip of oblique-reverse faults of the collective  
 616           Sargent and San Andreas faults by ; 4) Also, the 1989 coseismic elevation change with  
 617           uplift of uplifted 0.55 meters m on the southwestern hanging wall of the San Andreas and  
 618           Sargent faults, and subsidence of subsided 0.1 meters m on the northeastern footwall block  
 619           ; and 5) [Marshall *et al.*, 1991]. The thrusting was blind with the  $M_w$  7.1 earthquake not  
 620           being accompanied by coseismic, ground breaks—surface breaks. These aftershocks define  
 621           a conjugate pair of reverse faults with the dominant motion on the south-dipping fault  
 622           plane.

623           As in the 2010  $M_w$  7.0 Haiti earthquake, a secondary, blind thrust fault [Olson,  
 624           1990] beneath the surface trace of the Sargent fault that, and oblique to the main San An-  
 625           dreas strike-slip fault (shown in inset map of Figure 11), played a major role in the 1989  
 626           fault rupture and resulting pattern of regional uplift show shown in red color to the south-  
 627           west and regional subsidence shown in green-blue color to the northeast (Figure 11).

628           While the oblique thrust planes form smaller fault segments ranging in length from  
 629           3 to 11 km (Figure figure22A), the 2010 earthquake demonstrates that oblique thrusts  
 630           like the Léogâne fault are capable of producing a  $M_w$  7.0 earthquake with devastating re-  
 631           sults, especially when coupled with inadequate construction practices [Symithe and Calais,

632 2016]. Paleoseismic estimates of the age of the most recent deformation of Lake Azuey,  
 633 eastern Haiti, suggests that the latest activity of the EPGFZ in this area was in 1751 [Prentice  
 634 et al., 2010; Bakun et al., 2012]. Similar analysis indicates that the latest earthquake  
 635 event in the Lake Miragoâne area, western Haiti, was in 1770 [Bakun et al., 2012]. This ~~suggests~~  
 636 ~~the~~, ~~agreeing the previous study by~~ Bakun et al. [2012], ~~suggest the~~ earthquake recurrence  
 637 cycle along the EPGFZ is about 250 years. Therefore, in this transpressional setting, the  
 638 earthquake cycle may consist of an interplay between ruptures on the EPGFZ and ruptures  
 639 on the oblique thrusts and related folds.

640 The 2010  $M_w$  7.0 earthquake released part of the stress of the region, but as the  
 641 oblique thrusts may not be directly linked to the EPGFZ, it is possible that stresses on the  
 642 EPGFZ have continued to accumulate since the 18th century [Prentice et al., 2010]. Inte-  
 643 grated paleoseismic study of the EPGFZ with the commonly buried oblique thrust faults,  
 644 using geophysical and geologic methods, can help to inform the critical social issue of  
 645 how future earthquakes will be partitioned between the larger EPGFZ and other more ob-  
 646 scure, oblique faults

## 647 7 Conclusions

648 The main ~~conclusion~~ conclusions of the study are as follows:

649 1. ~~The devastating, 2010 Haiti earthquake ( $M_w$  7.0) was caused by rupture of the~~  
 650 ~~Léogâne blind, thrust fault located 5 km north of the main, Caribbean-Gonâve plate boundary:~~  
 651 ~~a 1200 km-long, left-lateral, Enriquillo-Plantain Garden fault zone (EPGFZ). Unexpectedly,~~  
 652 ~~the EPGFZ remained largely quiescent or slightly reactivated during the 2010 earthquake,~~  
 653 ~~although the EPGFZ formed a line of inflection between a coseismically uplifted lowland~~  
 654 ~~north of the EPGFZ and a subsided area in the highlands south of the fault.~~

655 2. ~~Here, we use high-resolution~~ High-resolution sonar data from two Haitian lakes  
 656 that straddle the EPGFZ and its northern flank ~~to demonstrate~~ demonstrates the presence  
 657 of a 10 – 15 km-wide, 120 km-long, late Holocene, fold-and-thrust belt, which is deform-  
 658 ing both the clastic lowland basins along the northern edge of the EPGFZ and the steep  
 659 topographic highlands to the south.

660 3. ~~2.~~ In the eastern part of the study area, sonar results from Lake Azuey show  
 661 that the EPGFZ is more deeply buried and less active than the adjacent, newly discov-  
 662 ered, northwest-striking, northeast-dipping Jimani thrust fault. This structural relation-

663 ship between the two faults is identical to the 2010 epicentral area 70 km to the west: the  
 664 2010 seismogenic, Léogâne blind thrust fault is northwest-to-east-striking, and the quies-  
 665 cent fault to the south during the 2010 earthquake is the east-west-striking, sub-vertical  
 666 EPGFZ.

667 **4–3.** The geographic distribution of 2010 aftershocks revealed that the seismogenic  
 668 motions of the Léogâne thrust fault and smaller motions on the EPGFZ terminated on a  
 669 similar northwest-striking fault: the submarine Trois Bains thrust fault. In the western-  
 670 most part of the study area, sonar results from Lake Mirogoâne show two overlapping and  
 671 active strands of the EPGFZ, and was instead diverted onto the Trois Bains thrust fault.

672 **5–4.** Our survey confirmed the pull-apart origin of Lake Mirogoâne and the lack  
 673 of historical deformation on this western segment of the EPGFZ during the 2010  $M_w$  7.0  
 674 earthquake. Integration of the geologic data across the study area show an alternation in  
 675 dip along nine northwest-striking, thrust faults at spacing of 5 to 40 km.

676 **6–5.** We interpret this zone of late Holocene deformation in clastic basins north of  
 677 the EPGFZ as the accommodation of transpressional strain supported by highly-oblique  
 678 GPS vectors across the study area. In this transpressional zone, coseismic deformation  
 679 alternates at recurrence intervals of centuries between oblique shortening structures, such  
 680 as Léogâne thrusts, Jimani thrusts, and Trois Bains thrusts, and strike-slip ruptures along  
 681 the narrow and well defined main trace of the EPGFZ.

682 **6. Our results, including the eastward extension of the EPGFZ into Dominican Republic,**  
 683 **support the “thick-skinned” strike-slip model along a 10–15 km-wide corridor of left-lateral**  
 684 **shearing centered on the EPGFZ as opposed to the southwestward propagation of the**  
 685 **Trans-Haitian fold-and-thrust belt proposed by Pubellier et al. [2000].**

## 686 Acknowledgments

687 We would like to thank the Society of Exploration Geophysicists’ Geoscientists Without  
 688 Borders program for supporting this project along with our earlier shallow-geophysical  
 689 imaging of the epicentral region on the Léogâne fan [Kocel et al., 2016]. We also express  
 690 our appreciation to Alex von Lignau (Haiti Department of Finance), Alfredo Lo Cicero  
 691 (Oxfam Italia in Haiti) for financial and logistical support on Lake Azuey. Ludner Re-  
 692 marais, and Jean Robert Altidor of the Haiti Bureau of Mines and Energy for their assis-  
 693 tance with fieldwork, permissions, and importation of equipment. Eric Fielding of NASA

694 [Jet Propulsion Laboratory \(JPL\)](#)/Caltech for kindly providing the [INSAR-InSAR](#) imagery.  
695 Roby Douilly of Purdue University for generously providing location information for after-  
696 shock data. We are grateful to Allied Geophysical Laboratories (AGL) and [WiH-William](#)  
697 Sager at University of Houston for assisting with equipment and fieldwork preparation.  
698 [Last but not least, we sincerely thank Jean-Francois Ritz, an anonymous reviewer, and](#)  
699 [Marc Jolivet, Tectonics Associate Editor, for their valuable comments and suggestions to](#)  
700 [improve the quality of the paper. The chirp sonar data used in this paper are available on](#)  
701 [AGL datastation \(<http://www.agl.uh.edu/resources-data.php>\) or by contacting the corresponding](#)  
702 [author.](#)

703 **References**

- 704 Bakun, W. H., C. H. Flores, and S. Uri (2012), Significant earthquakes on the Enriquillo  
 705 fault system, Hispaniola, 1500–2010: Implications for seismic hazard, *Bulletin of the*  
 706 *Seismological Society of America*, 102(1), 18–30.
- 707 Benford, B., C. DeMets, and E. Calais (2012), GPS estimates of microplate motions,  
 708 northern Caribbean: evidence for a Hispaniola microplate and implications for earth-  
 709 quake hazard, *Geophysical Journal International*, 191(2), 481–490.
- 710 Bien-Aimé Momplaisir, R. (1986), Contribution à l'étude géologique de la partie orientale  
 711 du Massif de la Hotte (Presqu'île du Sud d'Haïti): Synthèse structurale des marges de  
 712 la presqu'île à partir de données sismiques, *PhD thesis*, p. 210.
- 713 Bilham, R. (2010), Lessons from the Haiti earthquake, *Nature*, 463(7283), 878–879.
- 714 Bilham, R., and E. Fielding (2013), Remote sensing and the search for surface rupture,  
 715 haiti 2010, *Natural hazards*, 68(1), 213–217.
- 716 Bourgueil, B., P. Andreieff, J. Lasnier, R. Gonnard, J. Le Metour, and J.-P. Rancon (1988),  
 717 Synthèse géologique de la République d'Haïti, in *Technical report, Bureau des Mines et*  
 718 *de l'Energie*, Haiti Port-au-Prince.
- 719 Bruña, J. G., U. S. Ten Brink, A. Carbó-Gorosabel, A. Muñoz-Martín, and M. G. Balles-  
 720 teros (2009), Morphotectonics of the central Muertos thrust belt and Muertos Trough  
 721 (northeastern Caribbean), *Marine geology*, 263(1), 7–33.
- 722 Calais, E., Y. Mazabraud, B. Mercier de Lépinay, P. Mann, G. Mattioli, and P. Jansma  
 723 (2002), Strain partitioning and fault slip rates in the northeastern Caribbean from GPS  
 724 measurements, *Geophysical Research Letters*, 29(18).
- 725 Calais, E., A. Freed, G. Mattioli, F. Amelung, S. Jónsson, P. Jansma, S.-H. Hong,  
 726 T. Dixon, C. Prépetit, and R. Momplaisir (2010), Transpressional rupture of an un-  
 727 mapped fault during the 2010 Haiti earthquake, *Nature Geoscience*, 3(11), 794–799.
- 728 Calais, É., S. Symithe, B. M. de Lépinay, and C. Prépetit (2016), Plate boundary segmen-  
 729 tation in the northeastern Caribbean from geodetic measurements and Neogene geologi-  
 730 cal observations, *Comptes Rendus Geoscience*, 348(1), 42–51.
- 731 Chen, K.-C., B.-S. Huang, J.-H. Wang, and H.-Y. Yen (2002), Conjugate thrust faulting  
 732 associated with the 1999 Chi-Chi, Taiwan, earthquake sequence, *Geophysical Research*  
 733 *Letters*, 29(8).

- 734 Corbeau, J., F. Rolandone, S. Leroy, B. Meyer, B. Mercier de Lépinay, N. Ellouz-  
735 Zimmermann, and R. Momplaisir (2016), How transpressive is the northern Caribbean  
736 plate boundary?, *Tectonics*, 35(4), 1032–1046.
- 737 Cowgill, E., T. S. Bernardin, M. E. Oskin, C. Bowles, M. B. Yıldız, O. Kreylos, A. J.  
738 Elliott, S. Bishop, R. D. Gold, A. Morelan, et al. (2012), Interactive terrain visualization  
739 enables virtual field work during rapid scientific response to the 2010 Haiti earthquake,  
740 *Geosphere*, 8(4), 787–804.
- 741 Cox, B. R., J. Bachhuber, E. Rathje, C. M. Wood, R. Dulberg, A. Kottke, R. A. Green,  
742 and S. M. Olson (2011), Shear wave velocity-and geology-based seismic microzonation  
743 of Port-au-Prince, Haiti, *Earthquake Spectra*, 27(S1), S67–S92.
- 744 Dolan, J. F., H. T. Mullins, and D. J. Wald (1998), Active tectonics of the north-central  
745 Caribbean: Oblique collision, strain partitioning, and opposing subducted slabs, *SPE-  
746 CIAL PAPERS-GEOLOGICAL SOCIETY OF AMERICA*, pp. 1–62.
- 747 Douilly, R., J. S. Haase, W. L. Ellsworth, M.-P. Bouin, E. Calais, S. J. Symithe, J. G.  
748 Armbruster, B. M. de Lépinay, A. Deschamps, S.-L. Mildor, et al. (2013), Crustal struc-  
749 ture and fault geometry of the 2010 Haiti earthquake from temporary seismometer de-  
750 ployments, *Bulletin of the Seismological Society of America*, 103(4), 2305–2325.
- 751 Douilly, R., H. Aochi, E. Calais, and A. Freed (2015), Three-dimensional dynamic rupture  
752 simulations across interacting faults: The mw7. 0, 2010, haiti earthquake, *Journal of  
753 Geophysical Research: Solid Earth*, 120(2), 1108–1128.
- 754 Fielding, E. J., A. Sladen, Z. Li, J.-P. Avouac, R. Bürgmann, and I. Ryder (2013), Kine-  
755 matic fault slip evolution source models of the 2008 M7.9 Wenchuan earthquake in  
756 China from SAR interferometry, GPS and teleseismic analysis and implications for  
757 Longmen Shan tectonics, *Geophysical Journal International*, 194(2), 1138–1166, doi:  
758 10.1093/gji/ggt155.
- 759 Frankel, A., S. Harmsen, C. Mueller, E. Calais, and J. Haase (2011), Seismic hazard maps  
760 for Haiti, *Earthquake Spectra*, 27(S1), S23–S41.
- 761 Grindlay, N. R., M. Hearne, and P. Mann (2005), High risk of tsunami in the northern  
762 Caribbean, *Eos, Transactions American Geophysical Union*, 86(12), 121–126.
- 763 Hashimoto, M., Y. Fukushima, and Y. Fukahata (2011), Fan-delta uplift and mountain sub-  
764 sidence during the haiti 2010 earthquake, *Nature Geoscience*, 4(4), 255–259.
- 765 Hayes, G., R. Briggs, A. Sladen, E. Fielding, C. Prentice, K. Hudnut, P. Mann, F. Taylor,  
766 A. Crone, R. Gold, et al. (2010), Complex rupture during the 12 January 2010 Haiti

- 767 earthquake, *Nature Geoscience*, 3(11), 800–805.
- 768 Higuera-Gundy, A., M. Brenner, D. A. Hodell, J. H. Curtis, B. W. Leyden, and M. W.  
769 Binford (1999), A 10,300 14 C yr record of climate and vegetation change from Haiti,  
770 *Quaternary Research*, 52(2), 159–170.
- 771 Hornbach, M. J., N. Braudy, R. W. Briggs, M.-H. Cormier, M. B. Davis, J. B. Diebold,  
772 N. Dieudonne, R. Douilly, C. Frohlich, S. P. Gulick, et al. (2010), High tsunami fre-  
773 quency as a result of combined strike-slip faulting and coastal landslides, *Nature Geo-  
774 science*, 3(11), 783–788.
- 775 Kocel, E., R. R. Stewart, P. Mann, and L. Chang (2016), Near-surface geophysical investi-  
776 gation of the 2010 Haiti earthquake epicentral area: Léogâne, Haiti, *Interpretation*, 4(1),  
777 T49–T61.
- 778 Koehler, R., and P. Mann (2011), Field observations from the January 12, 2010, Haiti  
779 earthquake: Implications for seismic hazards and future post-earthquake reconnaissance  
780 investigations in Alaska, *Report of Investigations*, 2, 24.
- 781 Kroehler, M. E., P. Mann, A. Escalona, G. Christeson, et al. (2011), Late Cretaceous-  
782 Miocene diachronous onset of back thrusting along the South Caribbean deformed belt  
783 and its importance for understanding processes of arc collision and crustal growth, *Tec-  
784 tonics*, 30(6).
- 785 Leroy, S., N. Ellouz-Zimmermann, J. Corbeau, F. Rolandone, B. M. Lépinay, B. Meyer,  
786 R. Momplaisir, J.-L. Granja Bruña, A. Battani, C. Baurion, et al. (2015), Segmentation  
787 and kinematics of the North America-Caribbean plate boundary offshore Hispaniola,  
788 *Terra Nova*, 27(6), 467–478.
- 789 Lin, A., and T. Chiba (2017), Coseismic conjugate faulting structures produced by the  
790 2016 m w 7.1 kumamoto earthquake, japan, *Journal of Structural Geology*, 99, 20–30.
- 791 Mann, P. (1999), Caribbean sedimentary basins: Classification and tectonic setting from  
792 Jurassic to present, *Sedimentary Basins of the World*, 4, 3–31.
- 793 Mann, P., G. Draper, J. F. Lewis, et al. (1991), An overview of the geologic and tectonic  
794 development of hispaniola, *Geologic and tectonic development of the North America-  
795 Caribbean plate boundary in Hispaniola. Geological Society of America Special Paper*,  
796 262, 1–28.
- 797 Mann, P., F. Taylor, R. L. Edwards, and T.-L. Ku (1995), Actively evolving microplate  
798 formation by oblique collision and sideways motion along strike-slip faults: An example  
799 from the northeastern Caribbean plate margin, *Tectonophysics*, 246(1), 1–69.

- 800 Mann, P., E. Calais, J.-C. Ruegg, C. DeMets, P. E. Jansma, and G. S. Mattioli (2002),  
801 Oblique collision in the northeastern Caribbean from GPS measurements and geological  
802 observations, *Tectonics*, 21(6).
- 803 Marshall, G. A., R. S. Stein, and W. Thatcher (1991), Faulting geometry and slip from co-  
804 seismic elevation changes: the 18 October 1989, Loma Prieta, California, earthquake,  
805 *Bulletin of the Seismological Society of America*, 81(5), 1660–1693.
- 806 Massoni, P. (1955), *Haiti: reine des Antilles*, Nouvelles Editions Latines.
- 807 McHugh, C. M., L. Seeber, N. Braudy, M.-H. Cormier, M. B. Davis, J. B. Diebold,  
808 N. Dieudonne, R. Douilly, S. P. Gulick, M. J. Hornbach, et al. (2011), Offshore sedimentary effects of the 12 January 2010 Haiti earthquake, *Geology*, 39(8), 723–726.
- 809 Mercier de Lépinay, B., A. Deschamps, F. Klingelhoefer, Y. Mazabraud, B. Delouis,  
810 V. Clouard, Y. Hello, J. Crozon, B. Marcaillou, D. Graindorge, et al. (2011), The 2010  
811 Haiti earthquake: A complex fault pattern constrained by seismologic and tectonic ob-  
812 servations, *Geophysical Research Letters*, 38(22).
- 813 Moknatian, M., M. Piasecki, and J. Gonzalez (2017), Development of Geospatial and  
814 Temporal Characteristics for Hispaniola's Lake Azuei and Enriquillo Using Landsat  
815 Imagery, *Remote Sensing*, 9(6), 510.
- 816 Nettles, M., and V. Hjörleifsdóttir (2010), Earthquake source parameters for the 2010 Jan-  
817 uary Haiti main shock and aftershock sequence, *Geophysical Journal International*,  
818 183(1), 375–380.
- 819 Odonne, F., and P. Vialon (1983), Analogue models of folds above a wrench fault,  
820 *Tectonophysics*, 99(1), 31–46.
- 821 Olson, J. A. (1990), Seismicity in the twenty years preceding the loma prieta california  
822 earthquake, *Geophysical Research Letters*, 17(9), 1429–1432.
- 823 Paultre, P., É. Calais, J. Proulx, C. Prépetit, and S. Ambroise (2013), Damage to engi-  
824 neered structures during the 12 January 2010, Haiti (Léogâne) earthquake, *Canadian*  
825 *Journal of Civil Engineering*, 40(8), 777–790.
- 826 Piasecki, M., M. Moknatian, F. Moshary, J. Cleto, Y. Leon, J. Gonzalez, and D. Co-  
827 marazamy (2016), Report: Bathymetric Survey for Lakes Azuei and Enriquillo, His-  
828 paniola, *Tech. rep.*, City University of New York (CUNY).
- 829 Prentice, C., P. Mann, A. Crone, R. Gold, K. Hudnut, R. Briggs, R. Koehler, and P. Jean  
830 (2010), Seismic hazard of the Enriquillo-Plantain Garden fault in Haiti inferred from  
831 palaeoseismology, *Nature Geoscience*, 3(11), 789–793.

- 833 Prentice, C. S., P. Mann, F. Taylor, G. Burr, and S. Valastro (1993), Paleoseismicity of  
834 the north american-caribbean plate boundary (septentrional fault), dominican republic,  
835 *Geology*, 21(1), 49–52.
- 836 Pubellier, M., A. Mauffret, S. Leroy, J. M. Vila, and H. Amilcar (2000), Plate boundary  
837 readjustment in oblique convergence: Example of the Neogene of Hispaniola, Greater  
838 Antilles, *Tectonics*, 19(4), 630–648.
- 839 Rathje, E., J. Bachhuber, B. Cox, J. French, R. Green, S. Olson, G. Rix, D. Wells, O. Sun-  
840 car, E. Harp, et al. (2014), Geotechnical reconnaissance of the 2010 Haiti earthquake:  
841 GEER (Geotechnical Extreme Events Reconnaissance).
- 842 Rico, P. (2017), Hydrodynamic Study of Lake Enriquillo in Dominican Republic, *Journal*  
843 *of Geoscience and Environment Protection*, 5, 115–124.
- 844 Rios, J., C. McHugh, M. Hornbach, P. Mann, V. Wright, and D. Gurung (2013), Holocene  
845 activity of the Enriquillo-Plantain Garden Fault in Lake Enriquillo derived from seismic  
846 stratigraphy, in *AGU Fall Meeting Abstracts*, vol. 1, p. 2629.
- 847 Saint Fleur, N., N. Feuillet, R. Grandin, E. Jacques, J. Weil-Accardo, and Y. Klinger  
848 (2015), Seismotectonics of southern Haiti: A new faulting model for the 12 January  
849 2010 M7. 0 earthquake, *Geophysical Research Letters*, 42(23).
- 850 Segall, P., and M. Lisowski (1990), Surface displacements in the 1906 San Francisco and  
851 1989 Loma Prieta earthquakes, *Science*, 250(4985), 1241–1244.
- 852 Sibson, R. (2012), Reverse fault rupturing: competition between non-optimal and optimal  
853 fault orientations, *Geological Society, London, Special Publications*, 367(1), 39–50.
- 854 Sylvester, A. G. (1988), Strike-slip faults, *Geological Society of America Bulletin*, 100(11),  
855 1666–1703.
- 856 Symithe, S., and E. Calais (2016), Present-day shortening in Southern Haiti from GPS  
857 measurements and implications for seismic hazard, *Tectonophysics*, 679, 117–124.
- 858 Symithe, S. J., E. Calais, J. S. Haase, A. M. Freed, and R. Douilly (2013), Coseismic slip  
859 distribution of the 2010 M 7.0 Haiti earthquake and resulting stress changes on regional  
860 faults, *Bulletin of the Seismological Society of America*, 103(4), 2326–2343.
- 861 Taylor, F., P. Mann, S. Valastro Jr, and K. Burke (1985), Stratigraphy and radiocarbon  
862 chronology of a subaerially exposed Holocene coral reef, Dominican Republic, *The*  
863 *Journal of Geology*, 93(3), 311–332.
- 864 Terrier, M., A. Bialkowski, A. Nachbaur, C. Prépetit, and Y. Joseph (2014), Revision of  
865 the geological context of the port-au-prince metropolitan area, haiti: implications for

- 866 slope failures and seismic hazard assessment, *Natural Hazards and Earth System Sci-*  
867 *ences*, 14(9), 2577.
- 868 UNAVCO (University Navstar Consortium) (2009), PBO GPS velocities in southern Cali-  
869 fornia.
- 870 Wright, V. D., M. J. Hornbach, C. Mchugh, and P. Mann (2015), Factors contributing to  
871 the 2005-present, rapid rise in lake levels, dominican republic and haiti (hispaniola),  
872 *Natural Resources*, 6(08), 465.

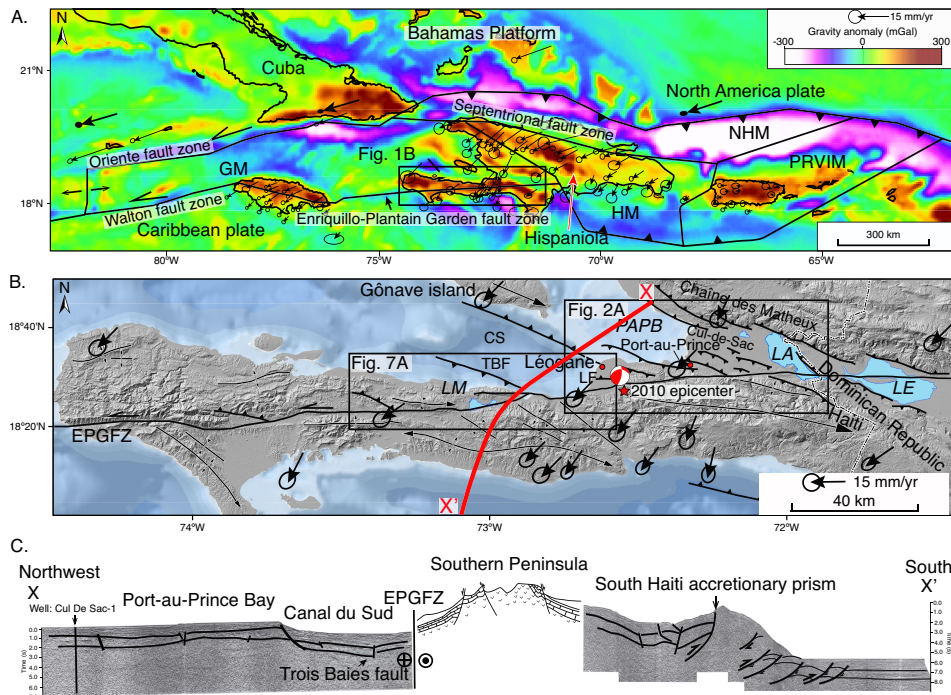
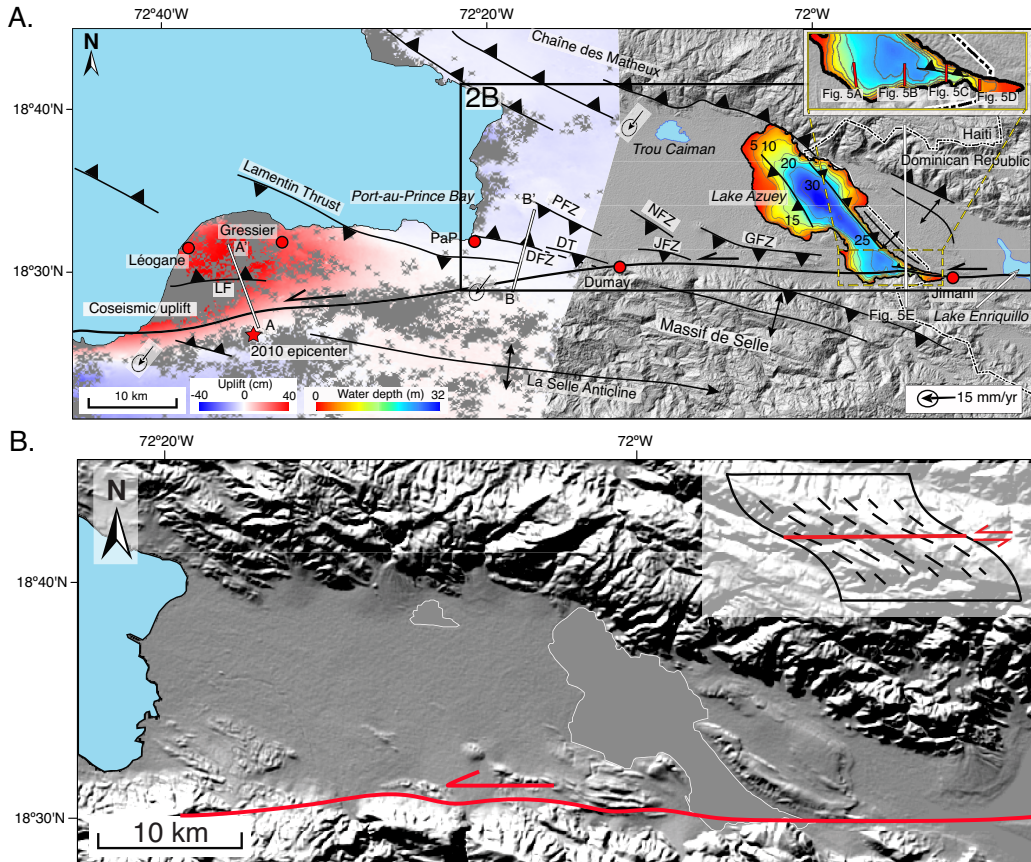
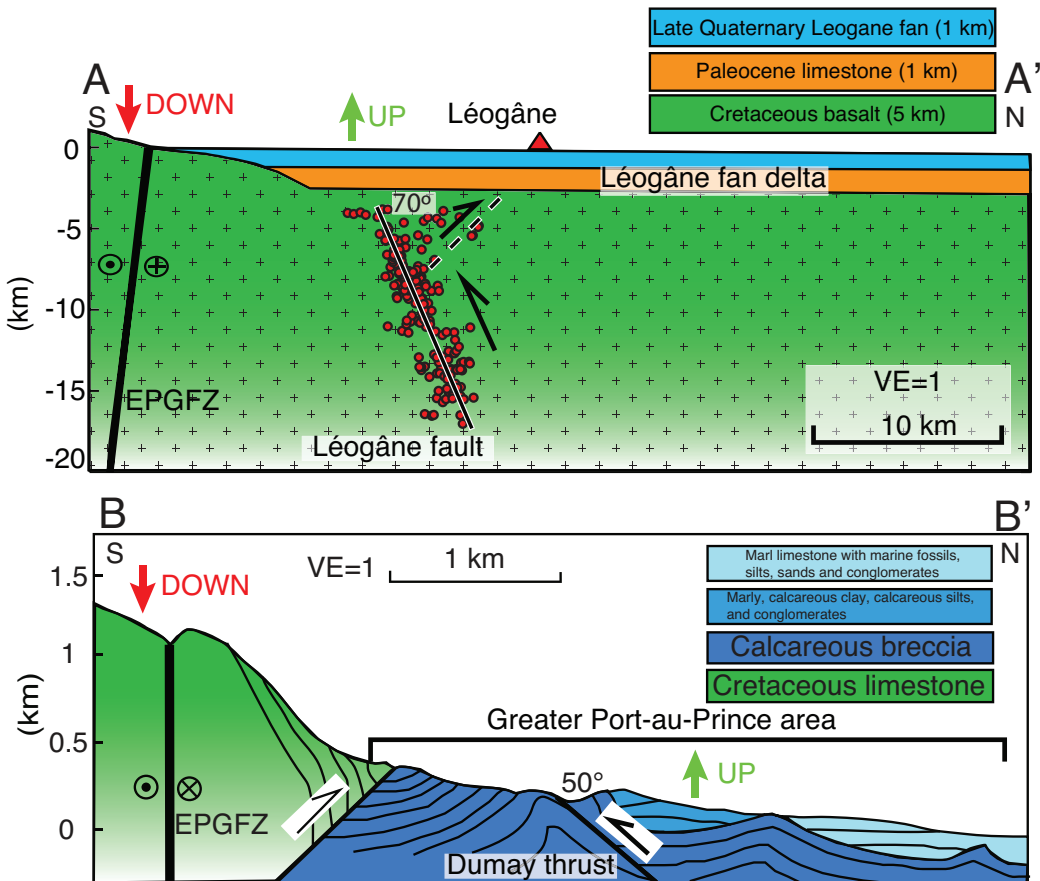


**Figure 1. Tectonic setting of the northeastern Caribbean and EPGFZ in southern Haiti. A:** Free-air gravity anomaly map of the Greater Antilles (Cuba, Jamaica, Hispaniola, Puerto Rico) in the northeastern Caribbean (<http://topex.ucsd.edu>) with gravity lows marking zones of subduction or thrusting along major faults (black lines) of the North America-Caribbean plate boundary. Arrows with error ellipses from *Calais et al. [2010]* are GPS vectors showing the direction and velocity of the large North American plate, the Bahamas carbonate platform (**BP**), and intervening microplates relative to a fixed Caribbean plate. Microplates with variable relative motions occupy the 200 km-wide plate boundary zone and include: **NHM** = North Hispaniola microplate; **HM** = Hispaniola microplate; **GM** = Gonâve microplate; **PRVIM** = Puerto Rico-Virgin Islands microplate. Box shows more detailed map of the EPGFZ shown in B. **B:** Regional structure map of the southern peninsula of Haiti with the active, left-lateral Enriquillo-Plantain Garden fault zone (EPGFZ) from the [Cul-de-Sac-Enriquillo basin-Lake Enriquillo](#) in the east to the [eastern-western](#) tip of the southern peninsula. [The centroid moment tensor \(CMT\) mechanism is from Douilly et al. \[2013\].](#) From east to west, key lakes and marine embayments aligned parallel and overlying the EPGFZ include: **LE** = Lake Enriquillo, Dominican Republic; **LA** = Lake Azuey, Haiti; **PAP PAPB** = Port-au-Prince Bay; **CS** = Canal du Sud; and **LA LM** = Lake Miragoâne; **LF** = Léogâne fault. Boxes shows more detailed maps of the structure of the EPGFZ and its secondary faults shown in Figure 2A and Figure 3A. **C:** Composite, multichannel seismic reflection line [from \(acquired by\)](#) Canadian Superior [Energy Inc.](#) located as the red line X-X' in B that shows an unfolded area of high-angle faults in the Canal du Sud tied to the offshore Cul-de-Sac-1 well, the TBFZ, the EPGFZ, the anticlinal structure of the southern peninsula, and a large, south-verging accretionary prism along the south coast of the southern peninsula. The depth scale for this section is in two-way, travel time.



893 **Figure 2. Structure of the EPGFZ in eastern Haiti. A:** Geologic faults and folds along a 15 km-wide  
 894 corridor parallel to the EPGFZ superimposed on a modified DEM and InSAR surface deformation map  
 895 (courtesy of Eric Fielding at JPL) [Hayes *et al.*, 2010]. Chirp bathymetry of the Lake Azuey is also shown.  
 896 GPS vectors are from Calais *et al.* [2010]. **PaP-T PFZ** = Port-au-Prince **thrust**fault zone; **DFZ** = Dumay **fault**  
 897 **zone**; **DT** = Dumay thrust; **NaC** = Nan Cadastre thrust; **Jac JFZ** = Jacquet **thrust**fault zone; **Gant-T GFZ**  
 898 = Ganthier **thrust**fault zone; **LF** = Léogâne fault. **Line A – A'**: Cross-section along the blind Léogâne thrust  
 899 fault (shown in Figure 3); **Line B – B'**: Cross-section of north Port-au-Prince urban area (shown in Figure 3).  
 900 **B:** Shaded DEM of the northern deformed belt in the Cul-de-Sac basin with illumination from the Figure 2A  
 901 showing *en echelon* and curvilinear folds *extending from north-northwest from striking west-northwest*  
 902 *obliquely with respect to* the EPGFZ and plunging beneath undeformed sediments occupying the center of the  
 903 Cul-de-Sac Valley. The inserted schematic diagram is from Odonne and Vialon [1983].

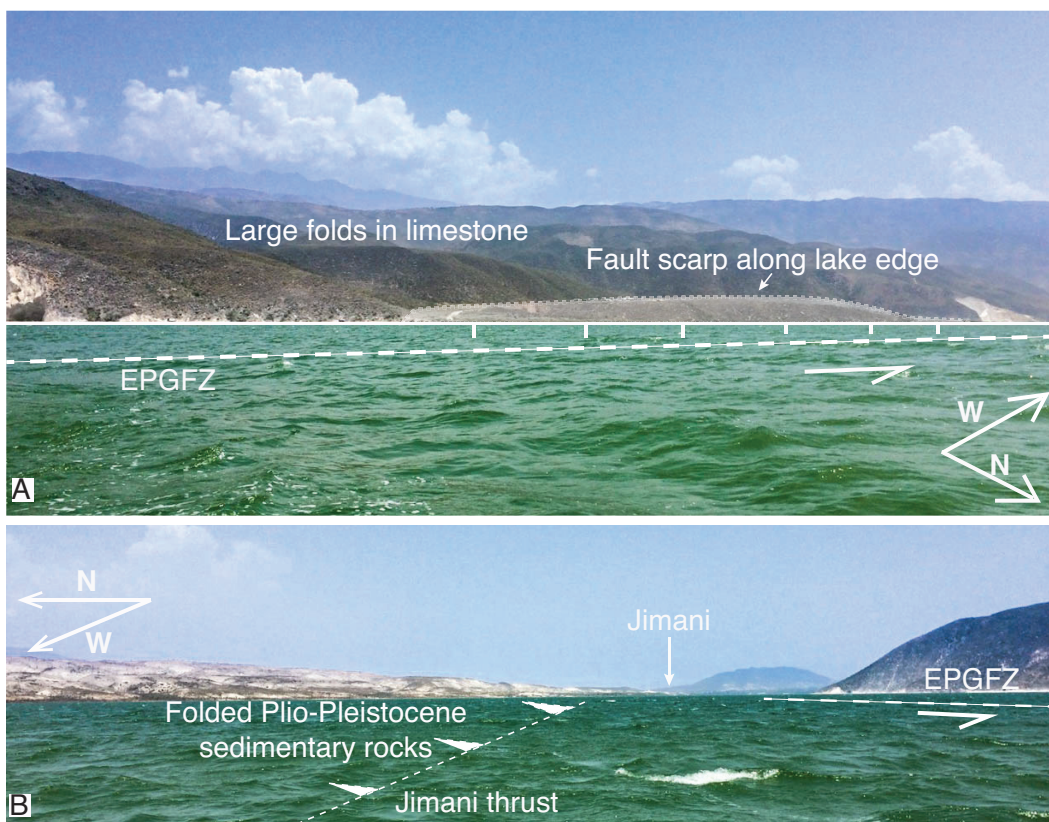
~



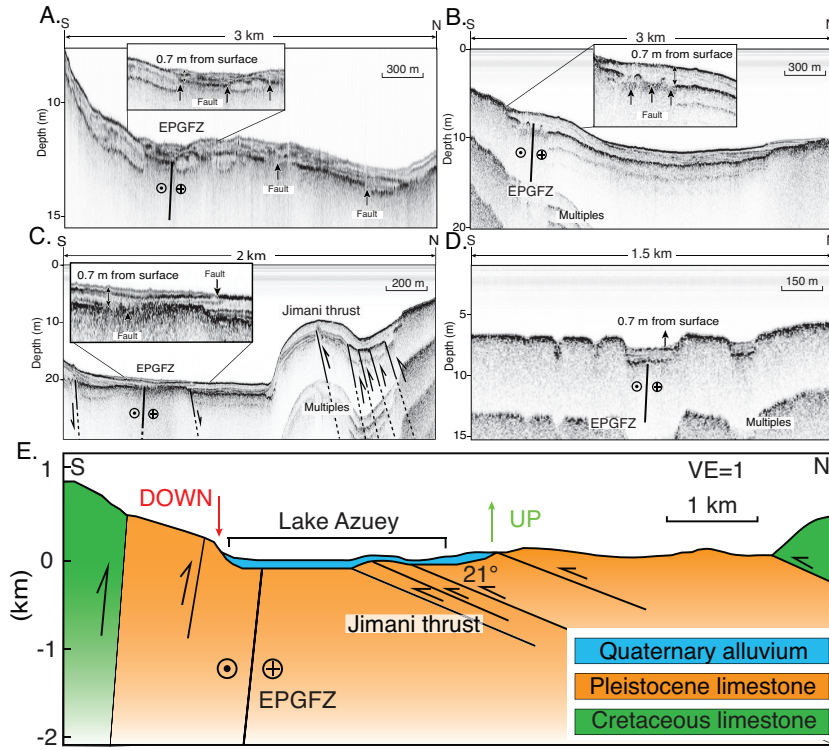
904 **Figure 3. Style of late Neogene deformation in the northern belt along three transects shown on the**  
 905 **map in Figure 2. Style of late Neogene deformation in the northern belt along three transects shown**  
 906 **in Figure 2. A-A':** Aftershocks of the 2010 earthquake [Douilly et al., 2013, 2015] along the blind Léogâne  
 907 thrust fault reveals conjugate reverse faults with the dominant slip occurring on the north-dipping fault. The  
 908 red triangle indicates Léogâne city. **B-B':** Cross section based on surface mapping  
 909 [Massoni, 1955; Cox et al., 2011; McHugh et al., 2011; Saint Fleur et al., 2015] showing north- and south-  
 910 dipping reverse faults deforming Plio-Pleistocene sedimentary rocks. **C-C':** Cross section based on both sonar  
 911 survey and the surface mapping showing north- and south-dipping, reverse faults deforming Plio-Pleistocene  
 912 sedimentary rocks.

**Structure of the EPGFZ in eastern Haiti and western-most Dominican Republic. A:**

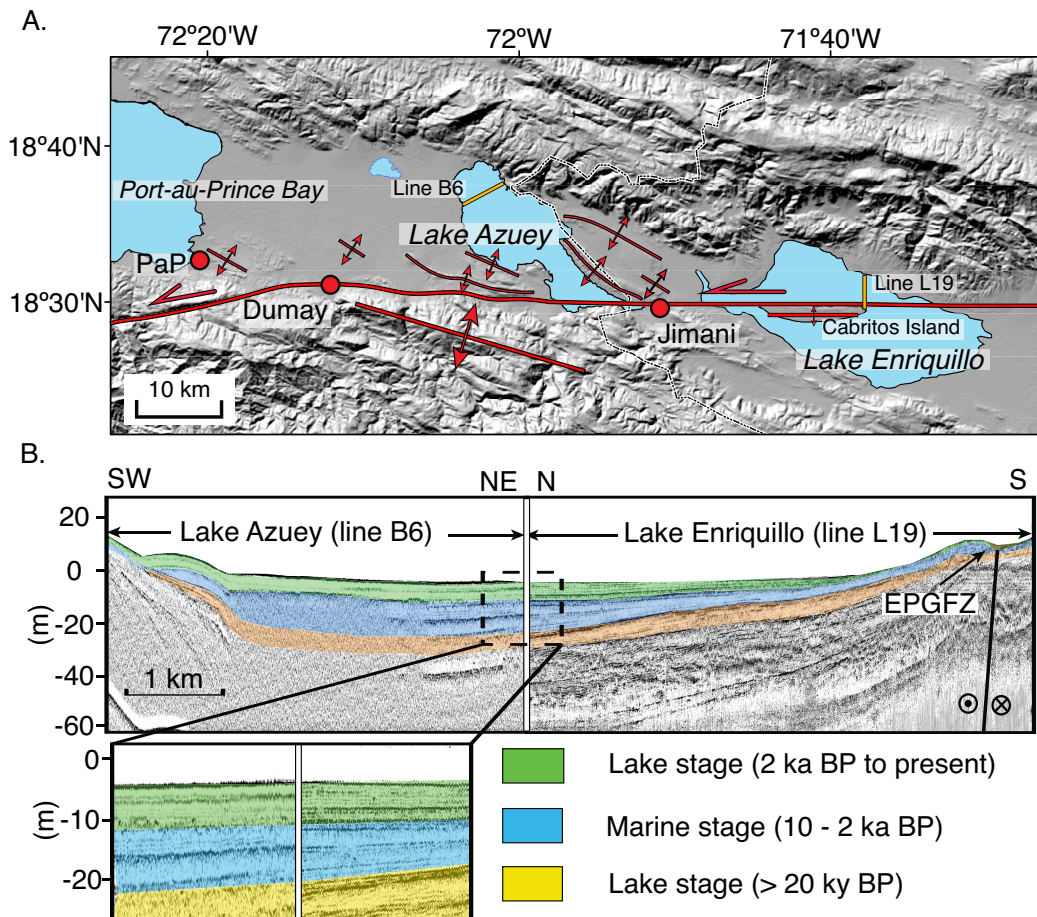
Structural map of Lakes Azuey and Lake Enriquillo with surfaces of 15 m ASL and 46 m BSL are presently separated by a shallow sill 30 m ASL in the isthmus near the town of Jimani. **B:** Comparison of two Chirp lines from Lake Enriquillo by (3 km-long Line L19) and from this own study of Lake Azuey (4 km-long Line B6). Identical sequences present on both lines suggest that the two lakes were once part of a single lake that has been recently separated by crustal movements related to the EPGFZ near the Jimani area. Ages of units are known from Lake Enriquillo through both exposures around the sub-sea level lake and from coring by.



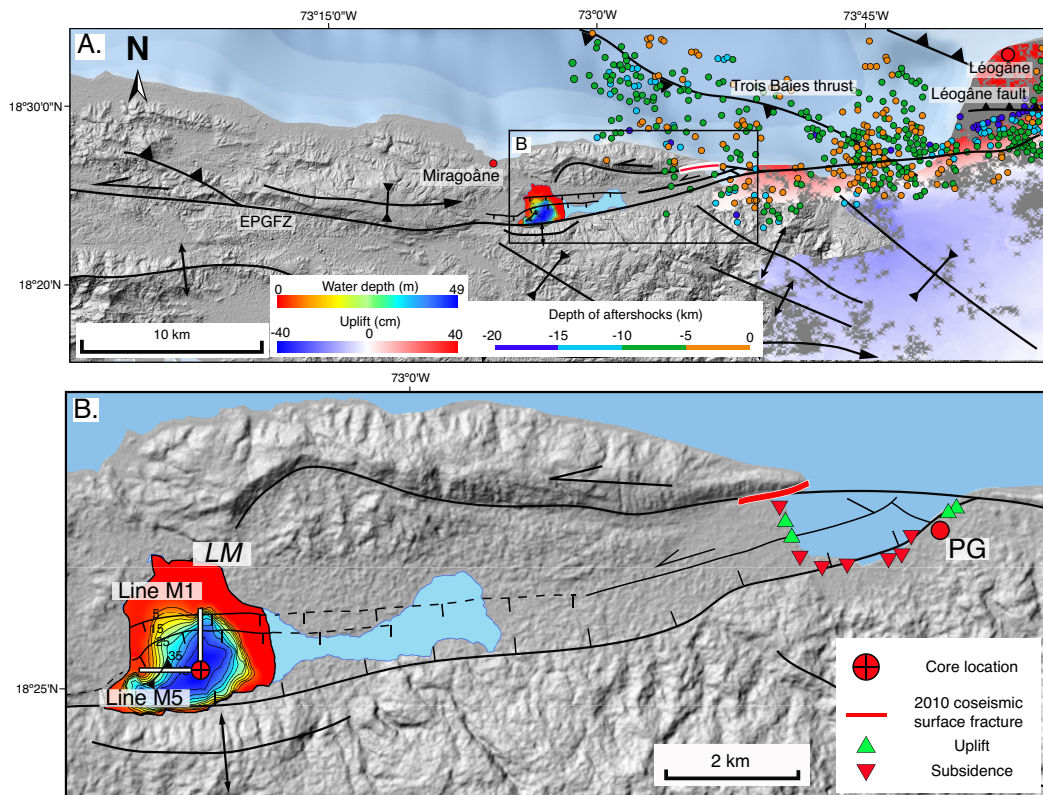
913 **Figure 4. Geologic setting of Lake Azuey, Haiti. A:** To the south, the green brackish waters of Lake  
914 Azuey are bound by the EPGFZ which forms a sharp boundary with 2 km-high, folded limestone of Paleo-  
915 gene age that forms the smooth surfaces on the skyline. One scarp is present along the edge of the lake while  
916 other parallel strands of the EPGFZ are beneath the southern part of the lake as schematically shown. **B:** To  
917 the north of the lake folded, Plio-Pleistocene strata form the uplifted, 0 – 30 m-high isthmus separating the  
918 two lakes. Approximate locations of the EPGFZ and the Jimani thrust fault are shown.



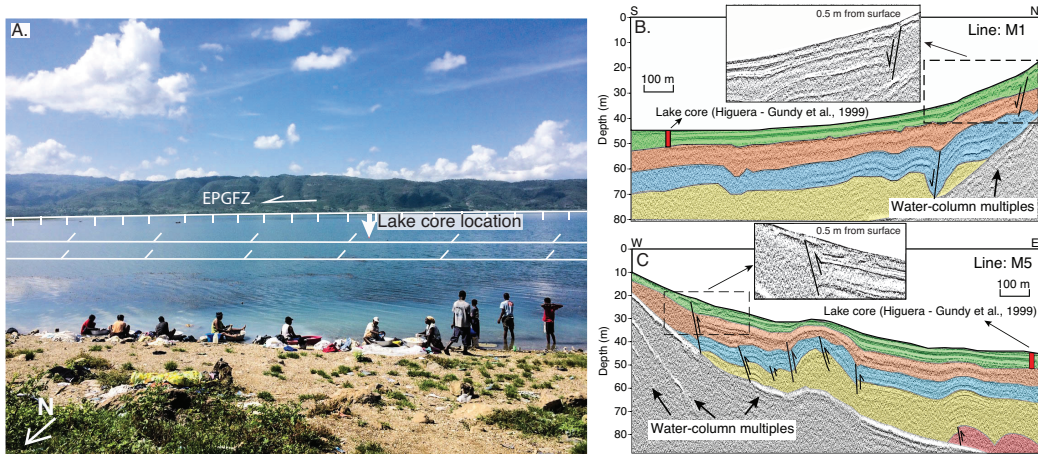
919 **Figure 5.** Chirp sonar profiles showing the relationship of the trace of the EPGFZ and a newly de-  
 920 scribed thrust we have named the Jimani thrust. Cross sections of A, and B are indicated in Figure 2A.  
 921 The EPGFZ beneath Lake Azuey forms a 10 m-wide zone that can be traced as a lineament to the east and  
 922 west of Lake Azuey (Figure 2). The green and red horizons represent two distinguish stratigraphic layers.  
 923 The two strands of the EPGFZ are buried by 0.7 m of Holocene sediment and are extrapolated to be **250**  
 924 **270** years old since their last rupture when a sedimentation rate of 2.6 mm/yr is assumed. Folds associate  
 925 with the Jimani thrust are interpreted as fault propagation folds. **C:** Cross section based on both sonar survey  
 926 and the surface mapping [Mann *et al.*, 1991] showing north- and south-dipping, reverse faults deforming  
 927 Plio-Pleistocene sedimentary rocks.



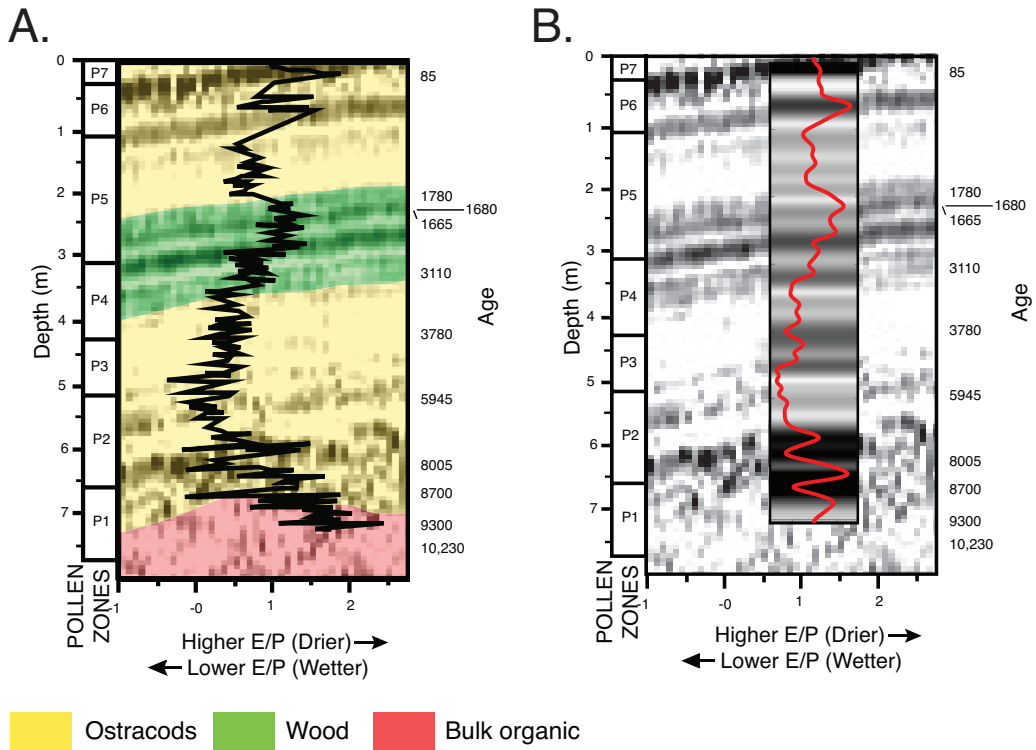
928 **Figure 6. Structure of the EPGFZ in eastern Haiti and western-most Dominican Republic. A:**  
 929 Structural map of Lakes Azuey (surface 15 m ASL) and Lake Enriquillo (surface 46 m BSL) are presently  
 930 separated by a shallow sill 30 m ASL in the isthmus near the town of Jimani. **B:** Comparison of two Chirp  
 931 lines from Lake Enriquillo by Rios *et al.* [2013] (3 km-long Line L19) and from our study of Lake Azuey (4  
 932 km-long Line B6). Identical sequences present on both lines suggest that the two lakes were once part of a  
 933 single lake that has been recently separated by crustal movements related to the EPGFZ near the Jimani area.  
 934 Ages of units are known from Lake Enriquillo through both exposures around the sub-sea level lake and from  
 935 coring by Rios *et al.* [2013].



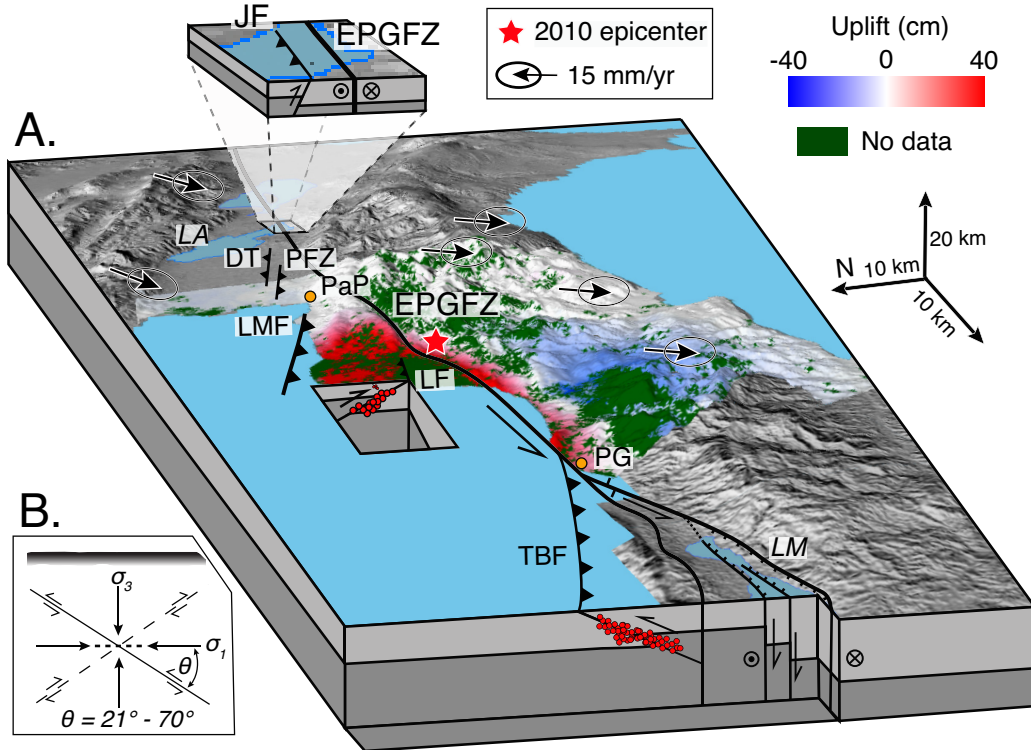
936 **Figure 7. Structure and 2010 coseismic surface deformation of the western segments of the**  
 937 **EPGFZ. A:** Structure [Prentice et al., 2010; Cowgill et al., 2012] and aftershock [Douilly et al., 2015]  
 938 [[Douilly et al., 2013](#)] map of Miragoâne-Léogâne region overlain with an InSAR image ([courtesy of Eric](#)  
 939 [Fielding at JPL](#)) [Hayes et al., 2010]. **B:** Zoom of the area of Petit Goâve and Lake Miragoâne showing the  
 940 structure and bathymetry of the 14 km<sup>2</sup>, pull-apart basin mapped beneath Lake Miragoâne during this study  
 941 and details of the 2010 surface fracturing and coseismic subsidence in the Petit Goâve Bay [Prentice et al.,  
 942 2010]. **LM** = Lake Miragoâne; **PG** = Petit Goâve.



943 **Figure 8. Geologic setting and sonar profiles from Lake Miragoâne.** **A:** View looking south across the  
 944 12 km-wide and 42.8 m deep, freshwater lake. The 2 km-high, ridge along the southern edge of the lake is  
 945 the cumulative topographic scarp ofassociated to the southernmost strand of the EPGFZ. The northern strand  
 946 of the EPGFZ is 3 km to the north of this strand and forms the northern edge of the pull-apart basin. The  
 947 core was taken by Higuera-Gundy et al. [1999] and was not collected from the deepest part of the lake. **B:**  
 948 **C:** North-south trending line M1 (location shown on Figure 7B). **C:** East-west trending line M5 (location shown  
 949 on Figure 7B).

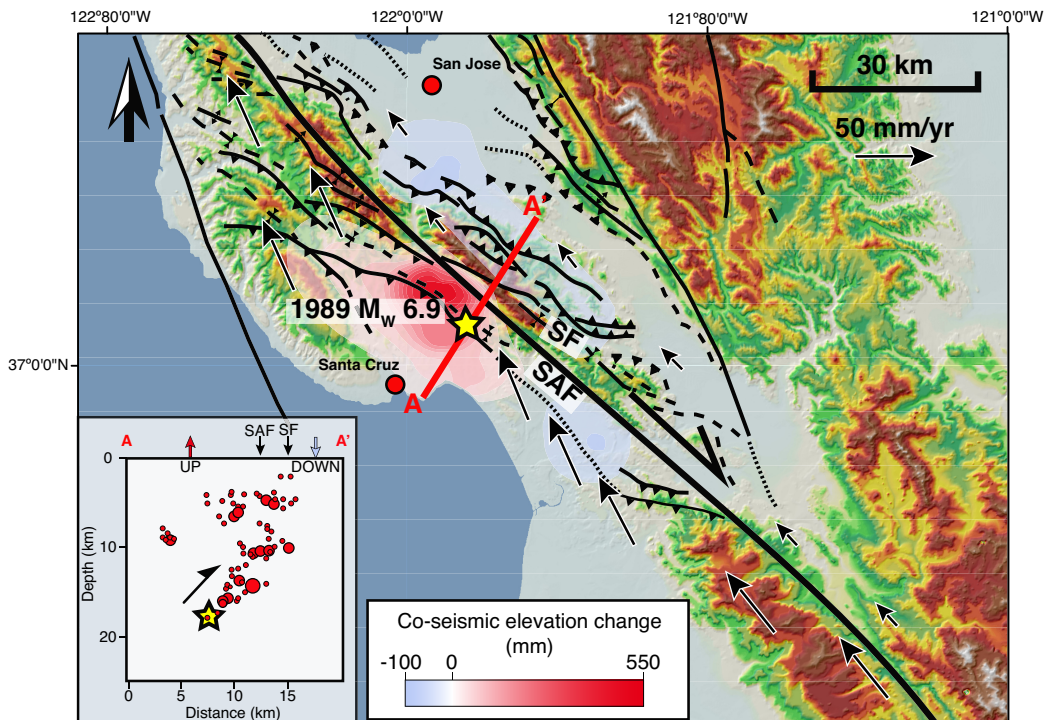


950 **Figure 9. Core data from Lake Miragoâne.** **A:** Tie between chirp sonar and core [Higuera-Gundy *et al.*,  
951 1999] extending to lacustrine sediments deformed by the EPGFZ at 1770 in 1770 A.D.. **B:** Low-pass filtered  
952 E/P log (red) and the synthetic sonar profile generated from the low-pass filtered E/P log used as an acoustic  
953 impedance. Red-The chirp sonar profiles are from the location of the red bar in the Figure 8A-B is the core  
954 measurement location, C.



955 **Figure 10. Three-dimensional block diagram showing the structural and aftershock expression of**  
 956 **late Holocene strain partitioning in a 40-km-wide zone along a 120 km-long segment of the EPGFZ.**  
 957 **Schematic diagram of the conjugate-thrust-fault model for the 10 – 15 km-wide belt of transpressional**  
 958 **deformation along the northern edge of the EPGFZ. A:** Three-dimensional block diagram showing the  
 959 **structural, aftershocks, and the late Holocene strain partitioning in a 40-km-wide zone along a 120 km-long**  
 960 **segment of the EPGFZ. Black arrows show southwest direction of the Gonâve microplate relative to the**  
 961 **Caribbean plate [and \[Calais et al., 2010\]](#). The 2010 InSAR-derived surface deformation map ([courtesy of](#)**  
 962 **[Eric Fielding at JPL](#) [Hayes et al., 2010]** show [and](#) a large component of shortening accommodated on a 40  
 963 **km-wide zone of oblique thrusts and folds north of the EPGFZ. PaP = Port-au-Prince; PG = Petit Goave;**  
 964 **LA = Lake Azuey; LM = Lake Miragoâne-Léogâne; JF = Jimani thrust fault; DT = Dumay thrust; PFZ =**  
 965 **Port-au-Prince fault zone; LMF = Lamartin thrust fault; TBF = Trois Baies thrust fault; LF = Léogâne fault.**

966 **B:** [The inserted schematic](#) Schematic diagram, modified from [Sibson \[2012\]](#), [represents](#), of the conjugate  
 967 [thrust faults.](#)



968 **Figure 11. Structural map of the San Francisco Bay region, the co-seismic elevation and the**  
 969 **aftershock cross-section of 1989  $M_w$  6.9 Loma Prieta earthquake. Structural map of the southern San**  
 970 **Francisco Bay region, the co-seismic elevation and the aftershock cross-section of 1989  $M_w$  6.9 Loma**  
 971 **Prieta earthquake. The selected GPS vectors relative to a fixed North America plate are from UNAVCO**  
 972 **(University Navstar Consortium) [2009]. The co-seismic elevation change and aftershock cross-section are**  
 973 **modified from Marshall *et al.* [1991]. SAF: San Andreas Fault; SF: Sargent Fault.**